Alma Mater Studiorum - Università di Bologna

DOTTORATO DI RICERCA IN

BIOLOGIA CELLULARE E MOLECOLARE

Ciclo 36

Settore Concorsuale: 05/I1 – GENETICA

Settore Scientifico Disciplinare: BIO/18 – GENETICA

METHYLATION OF PP2A AND ITS ROLE IN TRANSCRIPTIONAL REGULATION

Presentata da: Martina Gatto

Coordinatore Dottorato

Vincenzo Scarlato

Supervisore

Giovanni Perini

Co-supervisore

Alessandro Gardini

Esame finale anno 2024

Abstract

PPP2A (Proteins Phosphatase) is one of the most abundant phosphatases in cells. It consists of three subunits: A “scaffolding” subunit, C “catalytic” subunit and B “regulatory” subunit (which determines the function of PP2A). PP2A activity is influenced by the methylation occurring at Leucine 309 of the C subunit. LCMT1 (Leucin-methyltransferase 1) and PPME1 (Protein Phospho-methylesterase 1) are the proteins responsible for the methylation and demethylation of PP2A, respectively.

Recently it has been shown that PP2A can be recruited to the chromatin by interacting with Integrator, a 15-subunit complex involved in RNA Polymerase II transcription regulation. PP2A, along with the kinase CDK9, is responsible for phosphorylation/dephosphorylation of the CTD of RNA Polymerase II, which determines the transition from pause-release to productive elongation.

Although today we know how Integrator and PP2A interact with each other and how PP2A is recruited, we do not know yet when this binding occurs and how changes in PP2A methylation can affect RNA Polymerase II activity; hence, the main question to be addressed is: ***does the methylation status of PP2A affect transcription? How?*** Through a proteomic and genomic approach, I will try to convince you that yes, the methylation status of PP2A affects not only transcription but also some post-transcriptional events.

Index

Chapter 1: Introduction

Chapter 2: Results

Chapter 3: Methods

Chapter 1

Introduction

1.1 Transcriptional Regulation

Transcriptional regulation stands as a fundamental process governing the operation and growth of eukaryotic cells. Within the nucleus of every cell, the entire genome exists, yet only a specific subset of genes is actively expressed at any given moment. The precise timing and selective activation of these genes dictate the behavior and developmental trajectory of each individual cell. At the cellular level, the machinery responsible for transcribing DNA into RNA is highly conserved across species. This intricate process is orchestrated through specialized regulatory networks that ensure genes are turned on and off in a precisely coordinated manner. In eukaryotes, RNA Polymerase II is the complex responsible for the transcription of protein-coding genes (Washburn & Gottesman, 2015). The steps which the RNA Polymerase goes through are: initiation, elongation and termination. Each of them is regulated by various mechanisms and checkpoints. The initiation takes place by the time the RNA Polymerase II, helped by some transcription factors, binds the upstream of the gene (TSS). At this point, RNA Polymerase II is able to start to transcribe the RNA until the Polymerase activity stops (Moreno et al., 2023). The kinase CDK9 is able to phosphorylate some transcription factors and RNA Polymerase II C-terminal domain (CTD), allowing the RNA productive elongation. The transcriptional machinery is released from DNA once Polymerase II gets to the transcriptional end site (TES) (Tellier et al., 2022). At this point, the RNA undergoes maturation processes and is transported into the cytoplasm to be translated into protein (Xin Liu et al., 2013).

RNA Polymerase activity is regulated by some post-translational modifications occurring at the CTD, a highly conserved domain that consists of multiple heptad repeats (Tyr1–Ser2–Pro3–Thr4–Ser5–Pro6–Ser7) (Palancade & Bensaude, 2003) ,(Phatnani & Greenleaf, 2006), (Heidemann et al., 2013). Through the phosphorylation of most of these aminoacids, RNA Polymerase II is able to control gene expression (Schüller et al., 2016). More in detail, the phosphorylation of Serine 5

by CDK9 determines the begin of transcription, while the phosphorylation of Serine 2 allows the productive elongation after the RNA Polymerase II pause (Hsin et al., 2012) ,(Yu et al., 2015).

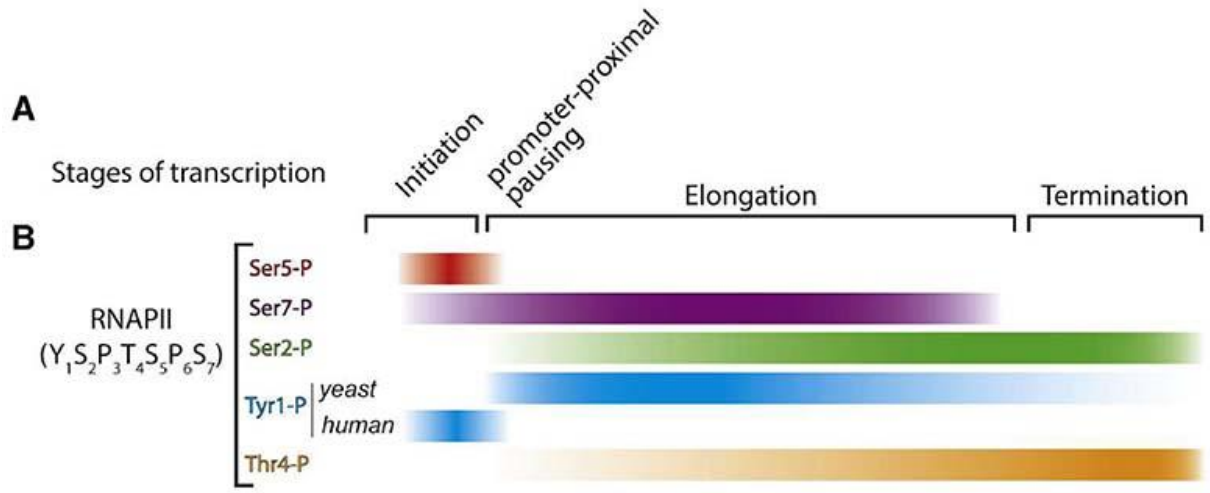

Figure. Pictures A and B provide a concise overview of the key stages of transcription and the importance of the C-terminal domain (CTD) phosphorylation of the largest subunit of RNA Polymerase II (RNAPII) in regulating these stages. Throughout the transcription cycle, the CTD undergoes differential phosphorylation, with distinct phosphorylation patterns at different stages of transcription. These phosphorylation patterns are indicated by colored bars and play a crucial role in facilitating the recruitment and exchange of stage-specific factors (Juan B. Rodríguez-Molina et al., 2023)

1.2 PP2A

Protein phosphorylation, a dynamic process, serves as a vital regulatory mechanism overseeing numerous cellular functions. This regulation hinges on the interplay between two opposing forces: protein kinases and phosphatases. These enzymes dictate the phosphorylation status of proteins, thus governing their activity and role within the cell. While more than 400 protein kinases are responsible for orchestrating the phosphorylation of serine and threonine residues, the task of dephosphorylation at these sites primarily falls upon ten catalytic subunits that comprise the Phosphoprotein Phosphatase family. This family encompasses the following members: PP1α, PP1β, PP1γ, PP2Acα, PP2Acβ, PP2Bc, PP4c, PP5c, PP6c, and PP7c. Together, they form a cadre of enzymes crucial for fine-tuning the intricate balance of protein phosphorylation within the cell,

thereby exerting precise control over various cellular processes (Scott P. Lyons, et al., 2021) (Guo et al., 2013).

PP2A (Protein Phosphatase 2A) is a critical serine/threonine phosphatase enzyme that plays a fundamental role in regulating various cellular processes, including cell growth, division, and signal transduction (Seshacharyulu et al., 2013). It is one of the major phosphatases in eukaryotic cells and is involved in the dephosphorylation of a wide range of substrates (Jiang et al., 2013) (Wlodarchak & Xing, 2016).

PP2A possesses a three-subunit structure comprising a catalytic unit denoted as 'C' (PP2A-C) (36 kDa), a scaffolding component referred to as 'A' (PP2A-A or PR65) (65 kDa), and a regulatory subunit 'B' (Figure 1A) (Xu et al., 2006). Both A and C subunits exist in two isoforms, α and β, respectively (Figure 1A) (Sablina & Hahn, 2007). In mammalian cells, A and C subunits are predominantly found in a complex form, forming AC dimers, also known as core dimers, or ABC trimers, referred to as heterotrimers or holoenzymes (Shi, 2009). A smaller fraction of these subunits may exist as 'free C' subunits, potentially stabilized through interactions with other regulatory proteins. PP2A B-subunits are broadly categorized into four families: (1) PPP2R2 (PR55 or B55), (2) PPP2R5 (PR61 or B56), (3) PPP2R3, and (4) STRN or Striatin (Figure 1A) (Amin et al., 2022). Each B-subunit subfamily includes approximately 3-5 different isoforms and additional splice variants, resulting in a total of at least 26 distinct B-subunits. Combinatorially, PP2A subunits can form close to 100 unique holoenzyme trimers (Wu, Chen, et al., 2017). These B-subunits are equipped with potential substrate-binding pockets and serve as regulatory partners whose binding guides specific PP2A complexes towards distinct sets of substrates, thus governing substrate specificity (Amanpreet Kaur et al., 2016).

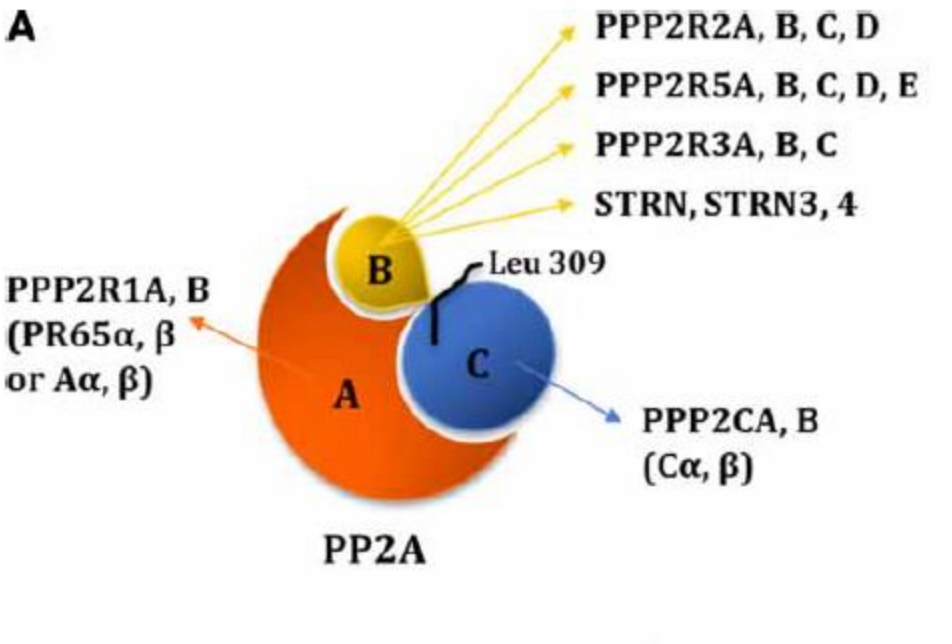

Figure 1. (A) PP2A complex with all isoforms of each subunit (Kaur & Westermarck, 2016).

PP2A is involved in the regulation of a wide range of cellular processes, including cell cycle progression, apoptosis, signal transduction, and cytoskeletal dynamics (Sents et al., 2013). It is a critical regulator of protein phosphorylation and functions in opposition to protein kinases, which phosphorylate proteins. By dephosphorylating specific substrates, PP2A helps maintain cellular homeostasis and prevent uncontrolled cell growth (Janssens et al., 2005).

PP2A is regulated by many protein interactions and post-translational modifications, such as two phosphorylations (T and Y) and one methylation (L) occurring at the C terminal of the catalytic subunit (^{304}TPDYFL^{309}) (Fig. 2B). Very little is known about phosphorylation, while the methylation occurring at Leucine 309 is the modification that has been studied the most. This methylation is regulated by the activity of two proteins which can add and remove the methyl group from the leucine: LCMT1 (Leucin-carboxyl-methyl-transferase1) and PPME1 (Protein Phosphatase Methyl-Esterase 1) (Kaur & Westermarck, 2016) (Stanevich, Jiang, Satyshur, et al., 2013).

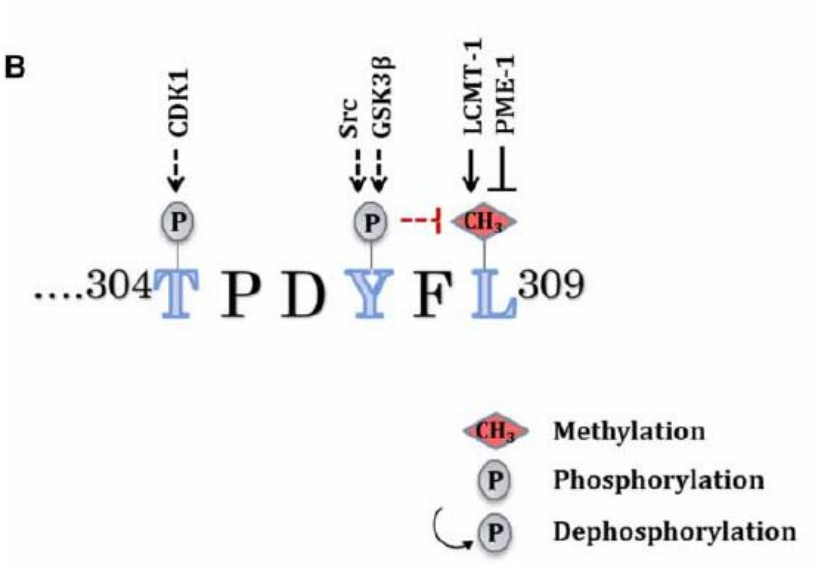

Figure 2. (B) Here is a simplified illustration of the possible posttranslational modifications of the PP2A-C subunit carboxy-terminal tail, with a focus on the role of LCMT-1 and PME-1 in methylation and demethylation of the Leu309 residue, as well as potential phosphorylation events at Thr304 and Tyr307. Phosphorylation of Tyr307 is shown to potentially inhibit the methylation of Leu309, indicated by the dotted red line (Kaur & Westermarck, 2016).

Beyond its role in hydrolyzing methylesters, PME-1 binding exerts an additional effect by diminishing the activity of PP2A (Yabe et al., 2018), (Li et al., 2022). This occurs through a process involving the rearrangement of the active site of PP2Acα and the displacement of the two essential divalent cations that are necessary for catalyzing the dephosphorylation reaction. This intricate interaction mechanism ultimately results in the reduction of PP2A catalytic activity. In cellular contexts, it is estimated that a significant portion of PP2Acα/β, specifically between 70% and 90%, undergoes methylation (Scott P. Lyons, et al., 2021) (Stanevich et al., 2014). The methylation status of PP2A determines the binding to certain B subunits (Wang et al., 2016). It's not clear yet which regulatory subunits prefer the methylated PP2A and which ones prefer the unmethylated PP2A (Tian et al., 2018), (Wu, Zheng, et al., 2017). Recent studies show that the regulatory B55 family preferentially binds to methylated PP2A, while all the others can bind both methyl-PP2A and unmethyl-PP2A (Longin S. et al., 2008; Yabe, R et al., 2018; Scott P. Lyons, et al., 2021).

In addition to its primary function as a methyl-esterase, PME-1 is proposed to act as a PP2A inhibitory protein by directly binding to the active site of PP2CA. This interaction further

underscores PME-1 role in modulating the activity of PP2A, suggesting a multifaceted regulatory mechanism involving both enzymatic and binding activities (Ryotaro Yabe et al., 2018) (Liu et al., 2015). Additionally, many other PP2A inhibitors have been discovered, such as SET and CIP2A (Dacol et al., 2021) which expression is elevated in cancers, causing the inhibition of PP2A activity (Amanpreet K., et al., 2016) (Kauko et al., 2020). (Liu et al., 2015) (Fig. 3 C).

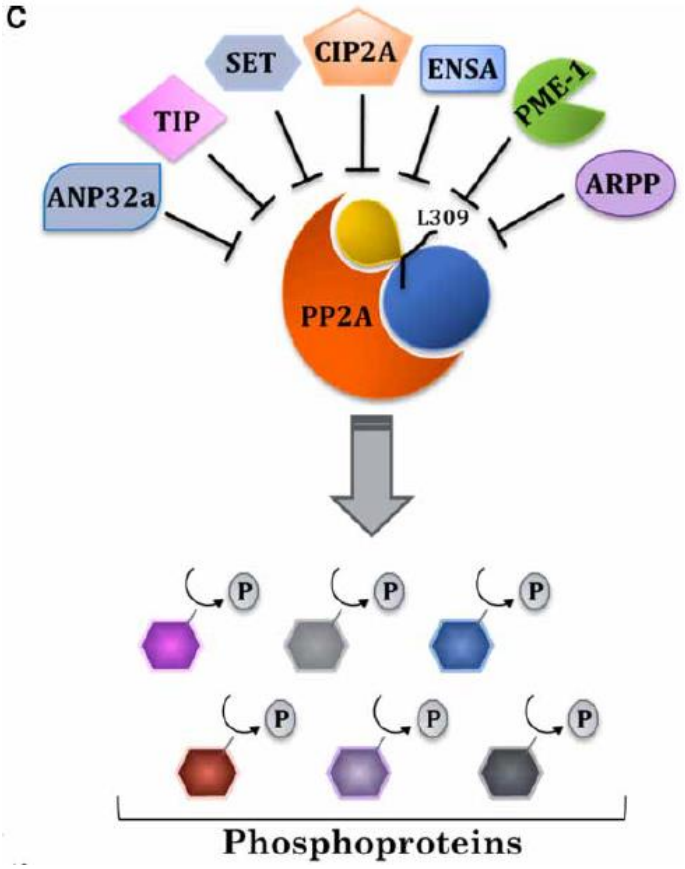

Figure 3. (C) PP2A complexes can be negatively regulated by cellular inhibitory proteins. These inhibitory proteins can hinder the activity of PP2A complexes, potentially leading to increased phosphorylation of their target proteins. Importantly, some of these inhibitory proteins are found to be highly expressed in cancer cells, contributing to the dysregulation of phosphorylation signaling networks. (Kaur & Westermarck, 2016)

1.3. The Integrator complex

In 2005, Integrator was unexpectedly discovered as a novel multi-subunit complex within human cells, demonstrating its ability to bind the RNA Polymerase II CTD. Through mass spectrometry analysis, researchers identified peptides originating from 12 previously uncharacterized open reading frames, associating them with several RNA Polymerase II subunits. Although orthologs for all these subunits were detected across metazoans, notably, they were absent in yeast, indicating the uniqueness of this complex to multicellular eukaryotes. Further exploration using sequence homology-based annotation tools unveiled an MBL/β-CASP region within Integrator complex subunit 9 (INTS9) and 11 (INTS11) (Lai et al., 2015). These regions bore a striking resemblance to cleavage and polyadenylation specificity factor subunit 73 (CPSF73; also known as CPSF3) and CPSF100 (also known as CPSF2), respectively. This discovery provided the initial indication that INTS9 and INTS11 might possess RNA endonuclease activity (Barbieri et al., 2018). Indeed, experiments involving the depletion of either the largest subunit (INTS1) or the presumed catalytic core (INTS11) of the Integrator complex resulted in the specific accumulation of unprocessed precursor U small nuclear RNAs (U snRNAs). As U snRNA processing is known to take place co-transcriptionally, this finding established a direct link between Integrator and the activity of Pol II (Kirstein et al., 2021).

Today we know that Integrator is constituted of 15 subunits (the last one “INTS15” was discovered in 2023) (Offley et al., 2023): INTS1, INTS2 and INTS7 form the central backbone of the Integrator complex. INTS3, besides being part of the Integrator complex, is also a member of the SOSS complex (along with NABP1, NABP2 and INIP) which is thought to recognize the ssDNA from DNA damage (Welsh & Gardini, 2023).

INTS4 has a homologue structure to symplekin in the CPSF complex and can form a stable trimeric complex with INTS9 and INTS11. Integrator is able to contact RNA Polymerase II (INTS1 binds RPB2, INTS7 and INTS2 can contact RPB3 and RPB11) and other transcription factors (INTS11 interacts with SPT5 and INTS6 with NELF-B) with most of its subunits (Fig. 4) (Gardini et al., 2014).

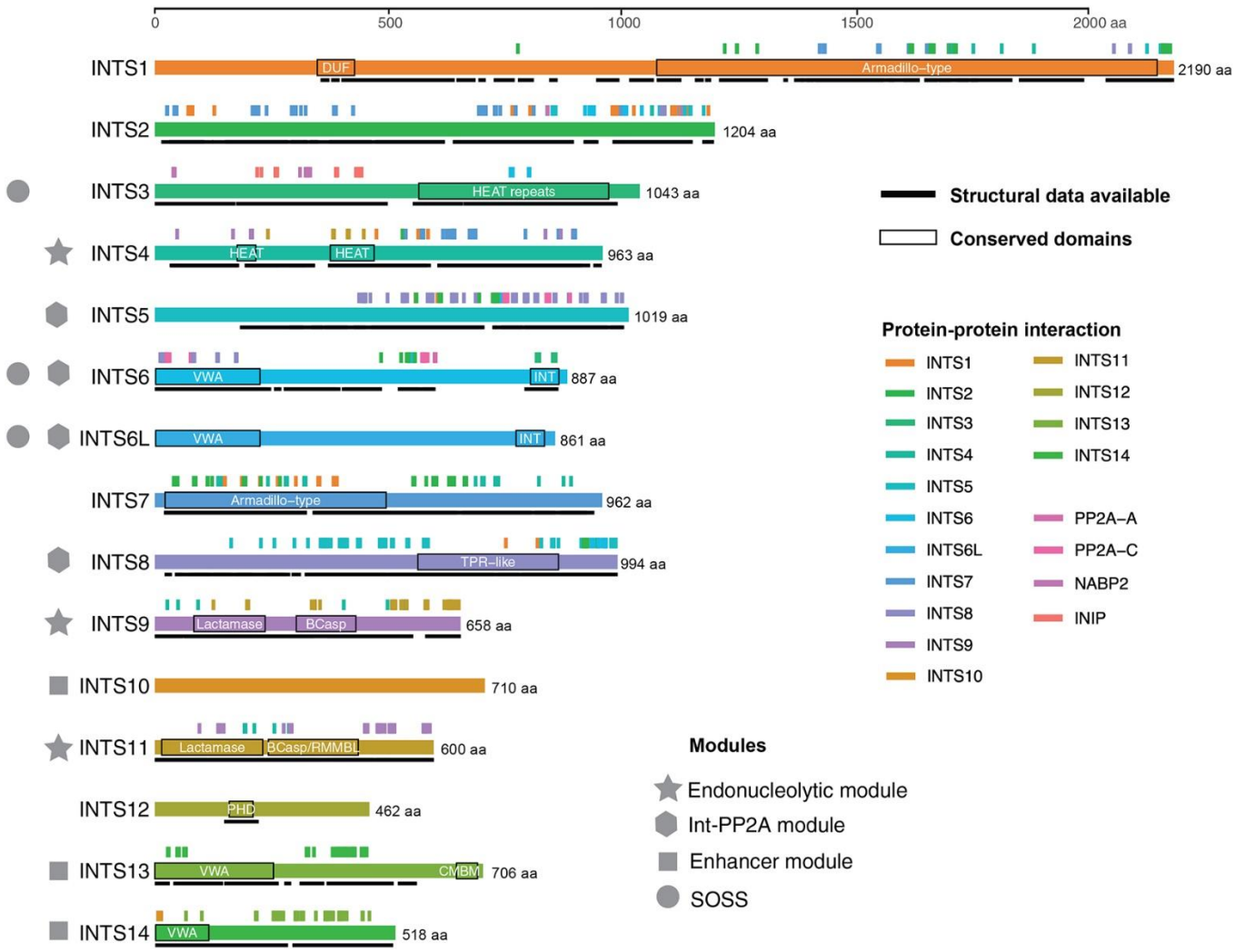

Figure 4. Structure of each Integrator subunit. (Welsh & Gardini, 2023)

The PP2A-INT complex (INTAC)

Recent studies have shown that PP2A and Integrator can assemble into a complex called INTAC. This complex is constituted of Integrator and PP2A dimer (subunit A and C) which structure suggests that INTAC is a catalytically active and noncanonical PP2A holoenzyme. The INTAC solved structure has shown that PPP2R1A subunit is bound to INTS8 while PPP2CA binds INTS6 (Zheng et al., 2021) (Fig. 5). INTAC complex binds RNA Polymerase II and dephosphorylates its CTD (Ser2 and Ser5) allowing, along with the kinase CDK9, the RNA Polymerase II 'pause-release' (Vervoort et al., 2021).

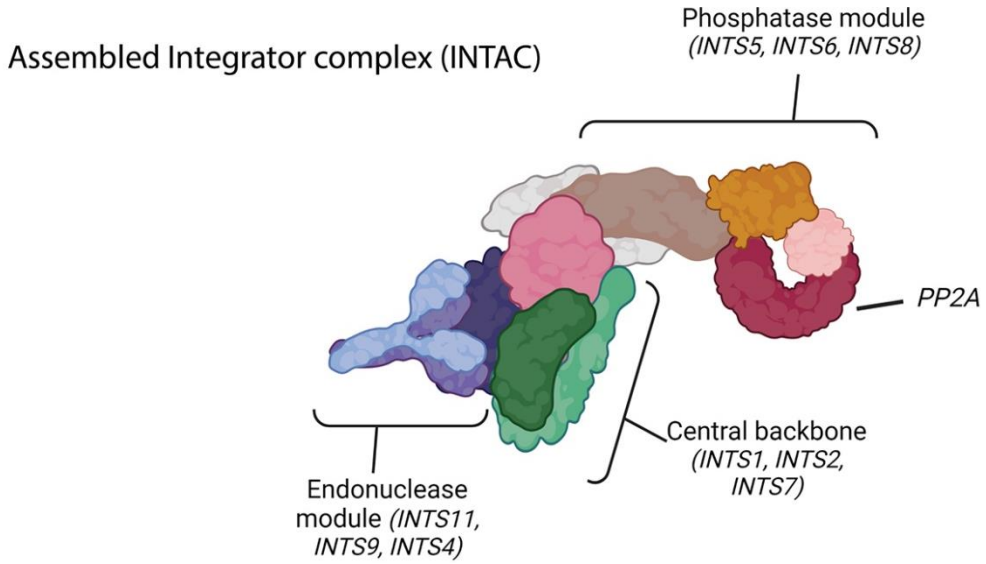

Figure 5. Integrator + PP2A (INTAC complex) (Welsh & Gardini, 2023)

Goals

In this thesis, I will present a series of experiments designed to uncover the significance of PP2A methylation in the regulation of transcription. Collectively, these experiments provide substantial evidence supporting the hypothesis that the methylation status of this phosphatase plays a pivotal role in determining PP2A activity not only during transcription but also in other cellular processes.

Chapter 2

RESULTS

PP2A Binding to INT and RNA Polymerase II is not affected by its methylation status

To directly assess PP2A methylation role in transcription, we decided to perform all experiments in two different cell systems: HeLa cells in which LCMT1 levels were decreased (short-term depletion, increase of unmethylated PP2CA)) and 293T cells in which LCMT1 levels were completely depleted (we got LCMT1 KO 293T and V2-293T parental cell line from Dr. Irfan Asangani's laboratory). We decided to work with these two different cell environments because we wanted to see if a quick and short change in PP2A methylation status could be compared to a well-established system lacking LCMT1. In some of the experiments I will show in my thesis, I will also perform a PPME1 short-term depletion (increase of unmethylated PP2A), in order to see if the decrease PPME1 can cause opposite effects to the ones seen after LCMT1 depletion.

To generate a short-term LCMT1 and PPME1 depletion, HeLa cells were infected with shLUC (Control), shLCMT1 and shPPME1 lentiviruses and selected for three days. Viral infection showed an evident decrease in LCMT1 and PPME1 (qPCR + WB) (Fig 1A-B-C). Moreover, there was a subsequential decrease of methylated PP2CA (shLCMT1) and unmethylated PP2A (shPPME1) levels both in nucleus and cytoplasm. PP2A methylation status is detected by 1D7 Biolegend antibody which is able to recognize the unmethylated form and by 7C10-C5 antibody (given by the Dr. Ogris's laboratory) which instead recognizes the methylated one (Frohner, Mudrak, Schüchner, et al., 2020), (Frohner, Mudrak, Kronlachner, et al., 2020) (Fig. 1D).

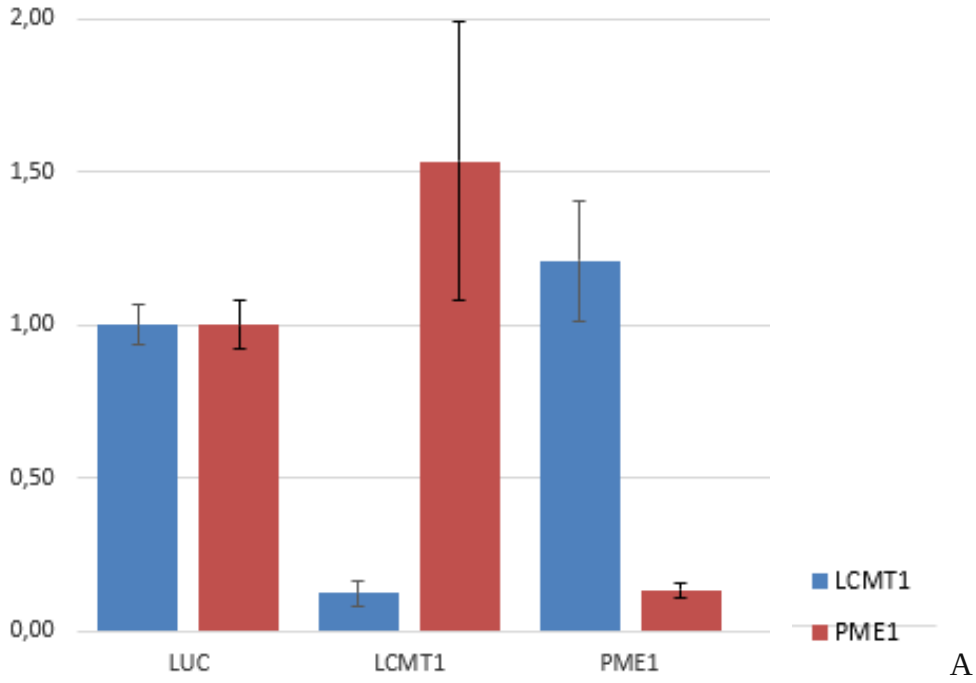
2,00
1,50
1,00
0,50
0,00
LUC
LCMT1
PME1
LCMT1
PME1

A

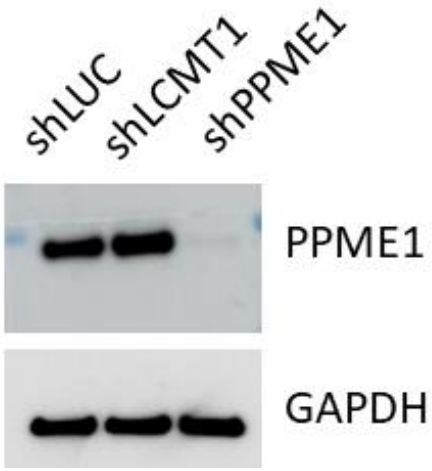
shLUC
shLCMT1
shPPME1
PPME1
GAPDH

B

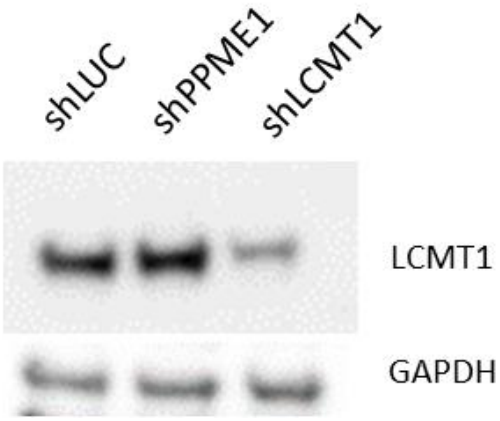
shLUC
shPPME1
shLCMT1
LCMT1
GAPDH

C

D

Figure 1. (A) The qPCR shows the reduction of LCMT1 and PPME1 RNA levels in shLCMT1 and shPPME1 samples, respectively. (B and C) The WB shows the reduction of LCMT1 and PPME1 protein levels in the nucleus in shLCMT1 and shPPME1 samples, respectively. (D) The WB shows PP2A methylation changes upon LCMT1 or PPME1 KD. In LCMT1 KD, it is possible to observe an increase of unmethylated PP2CA; instead, in PPME1 KD, there is an increase of methylated PP2CA. GAPDH shows that all samples have been loaded evenly.

From literature we know that PP2A methylation modification is able to change PP2A structure allowing the phosphatase to bind specific substrates. With this in mind, hence, once we assessed that effectively short-term decrease of LCMT1 was responsible for PP2A methylation status changes, we wondered if PP2A binding to RNA Polymerase II and Integrator could be affected by PP2A methylation changes. HeLa cells were infected with shLUC and shLCMT1 and selected for 3 days after lentiviral infection and then collected for nuclear extract. LCMT1 and methylated PP2A levels were checked by WB. 1.5 mg of shLUC and shLCMT1 nuclear extracts were incubated with 1D6 PP2CA antibody and beads A for 2h at 4℃ and Co-IP was performed. Protein immunoprecipitation was verified by WB and samples were digested by trypsinization for mass spectrometry (MS). To check Co-IP, we incubated membranes with INTS1, INTS6, PPP2R1A and PP2CA which are all subunits that are known to bind PP2A C catalytic subunit (Fig. 2A). MS data

showed that PP2CA is able to pull down the same number of peptides of Integrator and RNA Polymerase II subunits in both cellular systems (shLUC and shLCMT1), demonstrating that PP2A can be recruited to the chromatin regardless of its methylation status.

One significant revelation from the mass spectrometry analysis was that unmethylated PP2A (shLCMT1) appeared to exhibit a notably higher affinity for binding to PPP2R5C, PPP2R5D (both belonging to B56 family) and PPP2R2D (B55 family) B subunits compared to its methylated counterpart (shLUC). The Striatin 4 (STRN4) is the only one that binds definitively the methylated isoform (Fig. 2B). This finding represents a novel discovery, as existing literature had not previously demonstrated the preference of these B subunits for binding the unmethylated or methylated isoform. It appears that the other subunits do not exhibit a specific preference for a particular isoform. This pattern is consistent and observed not only in the nucleus but also in the cytoplasm (data not shown). One of the most recent papers (Lyons et al., 2021) has revealed that among all B subunit families, B55 family demonstrates a preference for the methylated PP2A isoform. According to this paper, the other families do not exhibit any such preference which is far from what I find in my experiments.

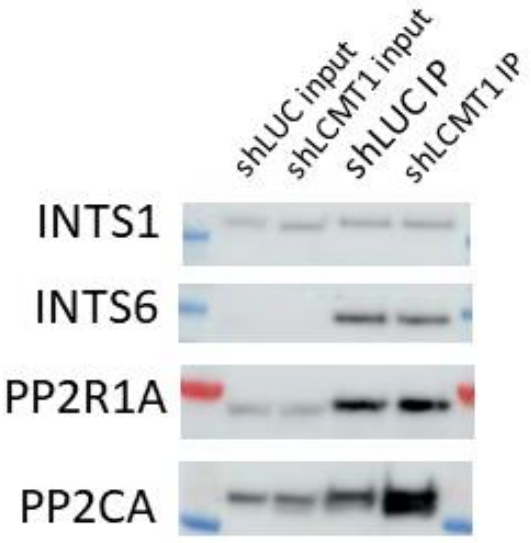

A

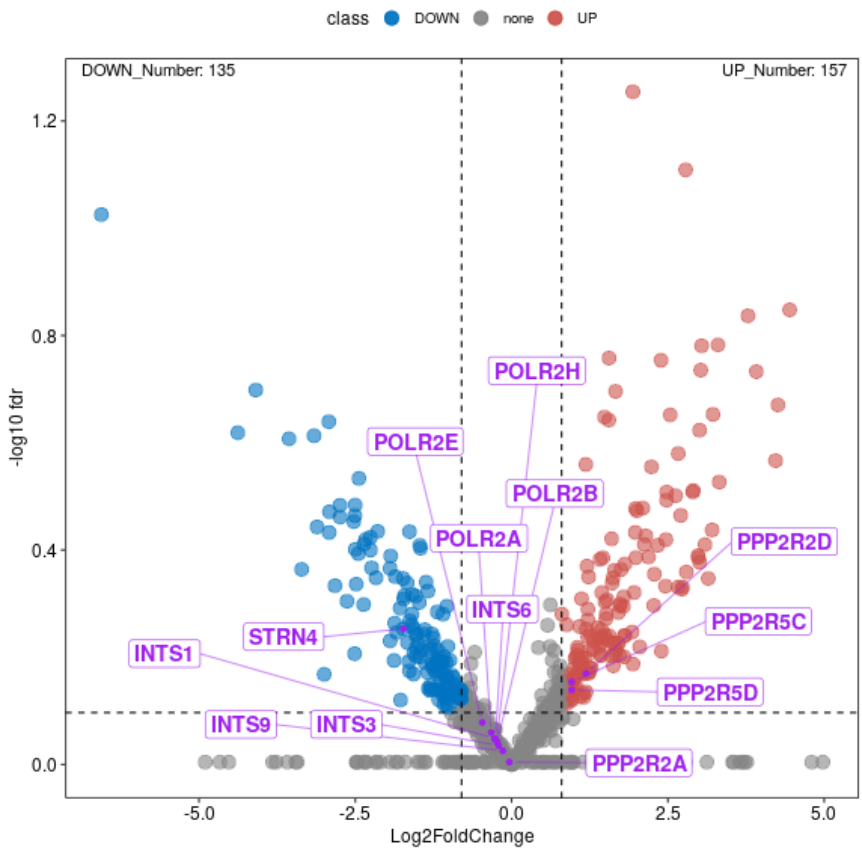

B

Figure 2. (A) 1D6 IP of shLUC and shLCMT1 nuclear extract + input. Membrane was incubated with INTS1, INTS6, PPP2R1A and PPP2CA antibodies. (B) The plot above represents the mass spectrometry data of 4 different shLUC – shLCMT1 PP2CA IPs replicates. Blue dots are all proteins binding more shLUC PP2CA, red ones are proteins binding strongly unmethylated PP2CA (shLCMT1). Proteins of interest (RNA Polymerase II, Integrator and B regulatory subunits) were labeled in purple. This plot suggests that there is no difference in their binding to PP2A, in fact most of them are grey dots (no significative p-value or foldchange). Some B subunit binding changes upon LCMT1 KD: PPP2R2D, PPP2R5C and PPP2R5D prefers unmethylated PP2A; STRN4 prefer the methylated isoform. The other B subunits are not shown because do not have any preferences.

All samples were normalized to PP2CA levels. IBAQ values were used to make the plot. Foldchange and p-value were obtained by Perseus software and graphbio was used to make the last figure.

Looking at all proteins interacting with PP2CA, it is also possible to observe that all Integrator subunits have a higher IBAQ than B subunit ones, demonstrating, hence, that in nucleus the

majority of PP2A is bound to Integrator rather than to the B subunits (fig.). Besides, all Integrator, canonical B subunits and PPME1, the plot shows IGBP1 (Immunoglobulin binding protein 1) which is known to be an essential regulator of PP2A phosphatase activity (Stanevich, Jiang, Sengupta, et al., 2013). IGBP1 binds PP2A with a balanced distribution way both in nucleus and cytoplasm with a stoichiometry similar to the Integrator one. This similarity implies that both IGBP1 and the Integrator complex may have complementary roles in regulating PP2A activity, possibly collaborating to fine-tune its functions (Kong et al., 2009) (Fig. 3).

Indeed, while the topic of IGBP1 may not be discussed in my current thesis, it is essential to acknowledge its significance, as it may open up avenues for further research and analysis in the future.

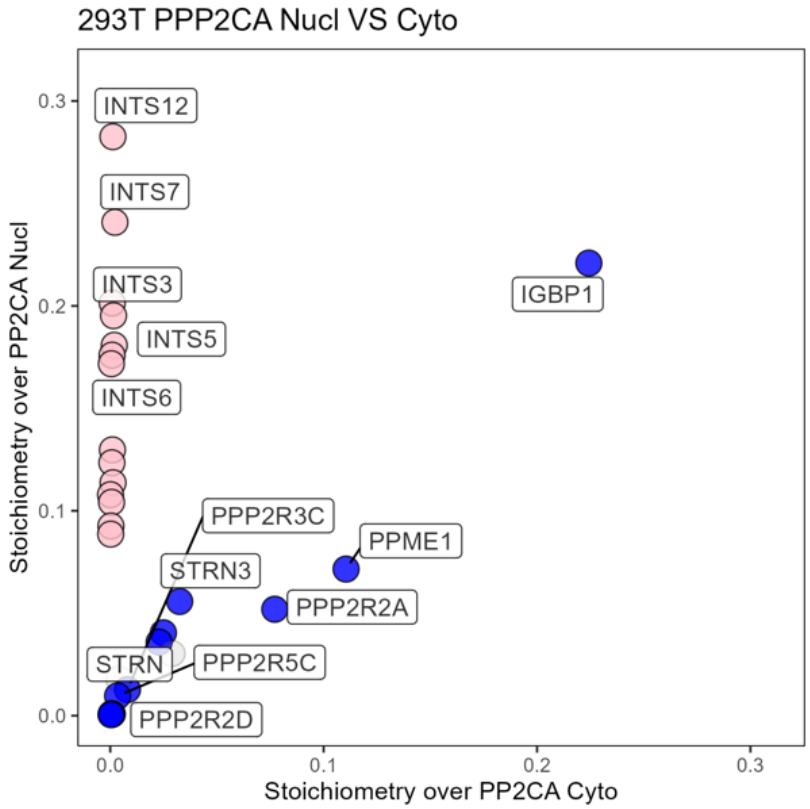

Figure 3. The plot represents the abundancy of INTS (pink dots) and B subunits/proteins belonging to PP2A complex (blue dots) binding PP2CA in nucleus (Y axis) and cytoplasm (X axis). In nucleus PP2CA binds many more Integrator subunits than B subunits. INT binding to PP2CA is between 1-100-fold higher than the B subunit one. In cytoplasm,

PP2CA does not bind any INT subunits. The stoichiometry is given by the iBAQ of each subunit divided by PP2CA iBAQ. IGBP1 is thought to be a protein able to activate/inactivate PP2A. PPME1 is the methyl-esterase responsible for the removal of the methyl group at Leu309 of C catalytic subunit.

WB and MS were also performed in 293T LCMT1 KO cells. As we expected, WB data showed that LCMT1 KO cells have higher levels of unmethylated PP2A and no methylated PP2A (Fig. 4). PPME1 levels do not change.

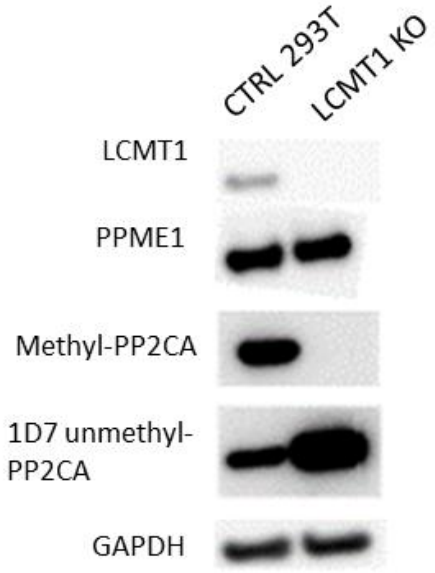

Figure 4. The WB shows LCMT1 KO effects on PP2A methylation: absence of methyl-PP2A and higher levels of demethylated PP2CA. No changes in PPME1 level. GAPDH control shows that samples have been loaded evenly.

MS data confirms what we observed in the short-term depletion: PP2A is recruited to the chromatin regardless of its methylation status, in fact both methylated and unmethylated PP2A can bind Integrator and RNA Polymerase II (Fig. 5). We obtained these results doing same experiments described before: we got nuclear extracts of WT 293T and LCMT1 KO 293T and performed Co-Immunoprecipitation (Co-IP) using 1D6 PP2A antibody. Elution was used to verify the Co-IP and for mass spec analysis.

The observation that both methylated and unmethylated PP2A can bind to Integrator and RNA Polymerase II on chromatin highlights that the role of PP2A in these processes is not solely dependent on its methylation status. The results from this recent experiment provide further confirmation of our earlier observations. Specifically, it confirms that in the absence of PP2A methylation, there is an increase in the binding of PPP2R5C and PPP2R5D in both the nucleus and cytoplasm (Fig. 5A - B) (Nasa & Kettenbach, 2020). Notably, in the knockout (KO) experiments, a new pattern emerges for another B subunit family, PPP2R3A (PR70 family), which shows an increased affinity for the unmethylated PP2A isoform. The observation that PPP2R2A shows a stronger binding affinity for methylated PP2A is consistent with findings in the existing literature and paper I mentioned earlier. Combining the findings from both the LCMT1 knockdown (KD) and LCMT1 knockout (KO) experiments, it becomes evident that, in general, most B subunits tend to exhibit a preference for a specific PP2A isoform. However, we can conclude that only two of these subunits (PPP2R5C and PPP2R5D) consistently demonstrate the same binding pattern in both the nucleus and cytoplasm in both LCMT1 KD and LCMT1 KO conditions.

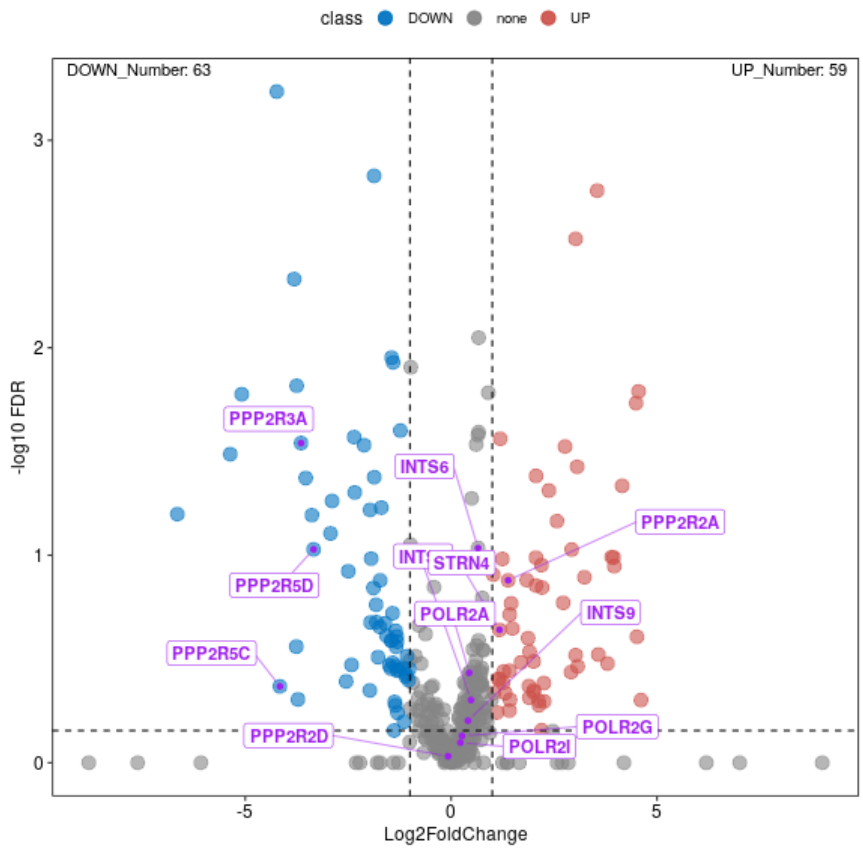
class DOWN none UP
DOWN_Number: 63
UP_Number: 59
-log10 FDR
Log2FoldChange
PPP2R3A
INTS6
PPP2R2A
STRN4
PPP2R5D
POLR2A
INTS9
PPP2R5C
POLR2G
PPP2R2D
POLR2I

A

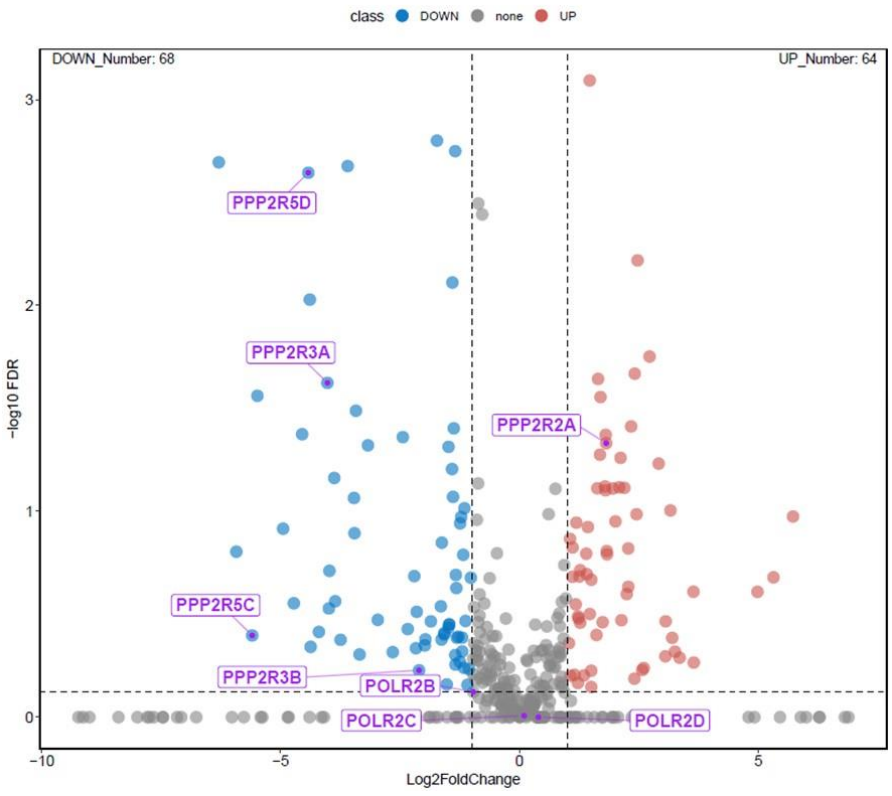
class DOWN none UP
DOWN_Number: 68
UP_Number: 64
-log10 FDR
Log2FoldChange
PPP2R5D
PPP2R3A
PPP2R2A
PPP2R5C
PPP2R3B
POLR2B
POLR2C
POLR2D

B

Figure 5. The plots above represent the mass spectrometry data of 3 different CTRL – LCMT1 KO PP2CA IPs replicates in nucleus (A) and cytoplasm (B). Blue dots are all proteins binding more LCMT1 KO unmethylated PP2CA, red ones are proteins binding strongly methylated PP2CA (293T WT). Proteins of interest (RNA Polymerase II, Integrator and B regulatory subunits) were labeled in purple. This plot shows that there is no difference in INT and RNA Polymerase II binding to PP2A in nucleus, in fact all those subunits are represented by grey dots (no significative p-value or foldchange). PP2A does not bind RNA Polymerase II in cytoplasm. On the contrary, B subunit binding changes: PPP2R5C, PPP2R5D and PPP2R3A binds unmethylated PP2A, while PPP2R2A the methylated isoform both in nucleus and cytoplasm.

Increase of CTD - Ser2 and Ser5 phosphorylation upon LCMT1 decrease

PP2A has been demonstrated to be able to bind the chromatin and dephosphorylate RNA Polymerase II CTD, antagonizing CDK9 phosphorylation activity. Despite both methylated and unmethylated PP2CA can bind Integrator and RNA Polymerase II, however, we thought that only one PP2A form is active and able to dephosphorylate RNA Polymerase II CTD and transcription factors (NELF and SPT5). First, we checked if the depletion of LCMT1 (increase of unmethylated PP2A) could affect RNA Polymerase II phosphorylation via WB (Fig. 6).

The concomitant increase in the phosphorylation of Serine 2 and 5 of the CTD of RNA Polymerase II in the nucleus when methylated PP2A levels decrease is a key finding. Phosphorylation at these sites is known to be crucial for transcription regulation, especially in the elongation phase. An increase in phosphorylation indicates that PP2A methylation is essential for the dephosphorylation of these specific sites on RNA Polymerase II CTD. The levels of total RNA Polymerase II and the scaffolding subunit PPP2R1A are not affected by LCMT1 depletion. This implies that the changes in Serine 2 and 5 phosphorylation are specifically related to the methylation status of PP2A, rather than changes in the abundance of these core transcription components.

The fact that these results were replicated in 293T LCMT1 KO cells highlights the robustness of our findings and suggests that LCMT1 impact on RNA Polymerase II CTD phosphorylation is not limited to a specific cell type (data not shown). The data from these knockout cells further support the idea that the loss of LCMT1, and the subsequent increase in unmethylated PP2A, directly

influences the phosphorylation state of RNA Polymerase II, specifically at Serine 2 and 5 of the CTD.

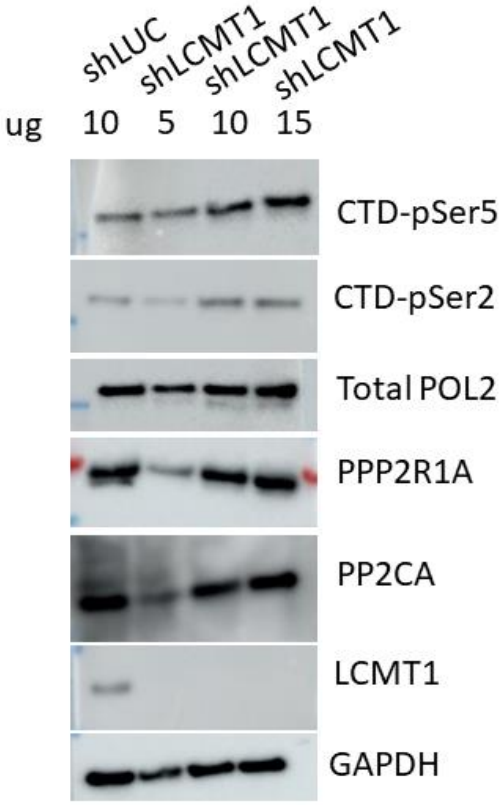

Figure 6. In this WB, different concentrations (5, 10, 15 ug) of nuclear shLCMT1 were loaded and membranes were incubated with different antibodies: CTD-pSer5, CTD-pSer2, Total RNAPII, PPP2R1A, PP2CA, LCMT1 and GAPDH (control). Comparing the lanes with same amount of extract (10 ug), we can observe an increase of CTD phosphorylation both at Ser2 and Ser5 in the LCMT1-depleted sample. PPP2R1A, Total RNA POL2 and PP2CA levels do not change.

To further establish changes in protein phosphorylation upon LCMT1 decrease, we decided to analyze the phosphorylation status of proteins via TiO_2 phosphoproteome enrichment. shLUC/shLCMT1 HeLa and WT/LCMT1 KO 293T samples obtained from nuclear extracts were dialyzed overnight and urea was added at high concentrations to allow the effective protein denaturation. Unfortunately, we were not able to detect a decent number of peptides in all replicates of HeLa LCMT1 knock down: low peptide recovery can lead to issues with statistical significance. 293T LCMT1 KO, on the contrary, had a better recovery of peptides even if

sometimes, p-values are not as high as we desired. The phosphoproteome enrichment techniques can vary depending on the complexity of the sample. HeLa and 293T cells may have different proteomes and phosphoproteomes, which could explain the differences in the results between the two cell lines. For all these reasons, we will just show LCMT1 KO phosphoproteome results. To perform the analysis, I first normalized samples to make the data more comparable. I determined the normalization factor by dividing the total sum of unique sites in LCMT1 KO samples by the sum of unique sites in CTRL 293T sample. In my example, this resulted in a normalization factor of 1.21, indicating that the LCMT1 KO sample had 1.21 times more unique sites compared to the control. The normalized values were then imported in Perseus and it allowed me to get p-value and foldchange, which were later used in R to get the actual plots.

The volcano plot shows that there are 9680 unique peptides that are hyper-phosphorylated in LCMT1 KO and 7679 that are hypo phosphorylated. The difficulty in detecting and recovering CTD peptides, likely due to their small size, is a common challenge in phosphoproteomics. However, the detection of increased CTD phosphorylation in one LCMT1 KO replicate aligns with our previous Western blot results, reinforcing the impact of LCMT1 on RNA Polymerase II phosphorylation (Fig. 7B). Given the challenges with CTD peptide, we decided to focus more on the other transcription factors that are known to be dephosphorylated by PP2A, such as NELF and SPT5 (Drouin et al., 2010), (Ohe et al., 2022). NELF is a complex (NELF-A, NELF-B, NELF-CD, NELF-E) that negatively regulates transcription elongation. It needs to be phosphorylated to allow productive transcription. Our volcano plot indicates that many residues in NELF-A, NELF-B, and NELF-E are more phosphorylated in the absence of LCMT1 (Fig. 7A). This finding suggests that LCMT1 plays a role in the dephosphorylation of NELF, which negatively regulates transcription elongation. An increase in NELF phosphorylation may affect its activity and potentially promote productive transcription.

SPT5 is a protein that positively regulates transcription and that has to be phosphorylated at Serine 666 to allow productive elongation. Our observation of the hyper-phosphorylation of SPT5 at Serine 666 upon LCMT1 depletion aligns with the expected outcomes based on our earlier findings. The detection of hyper-phosphorylation at this site (fold change of almost 5) in LCMT1-depleted samples suggests that LCMT1 has a role in controlling the phosphorylation status of SPT5 (Fig. 7B).

The collective results suggest that LCMT1, through its influence on RNA Polymerase II phosphorylation, has effects on transcriptional activity and on the phosphorylation of key transcription factors like SPT5 and NELF.

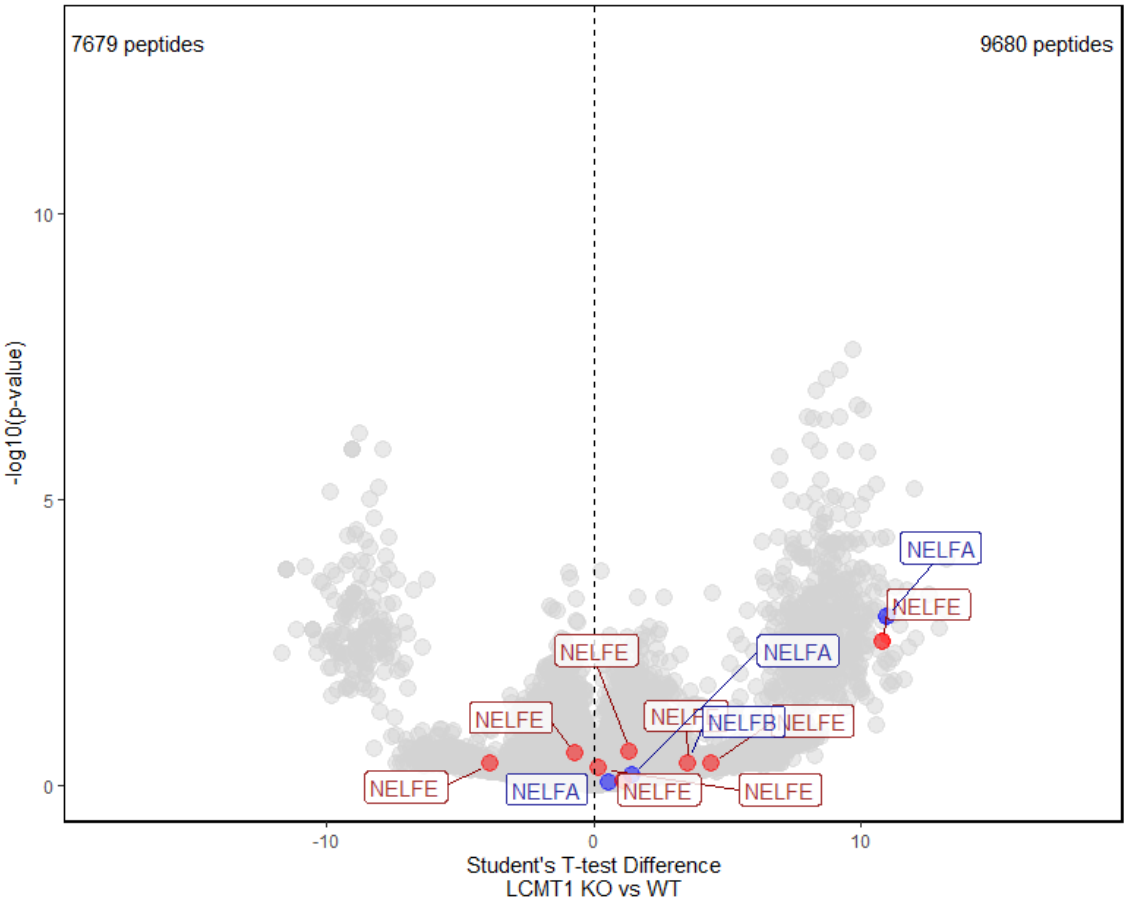

A

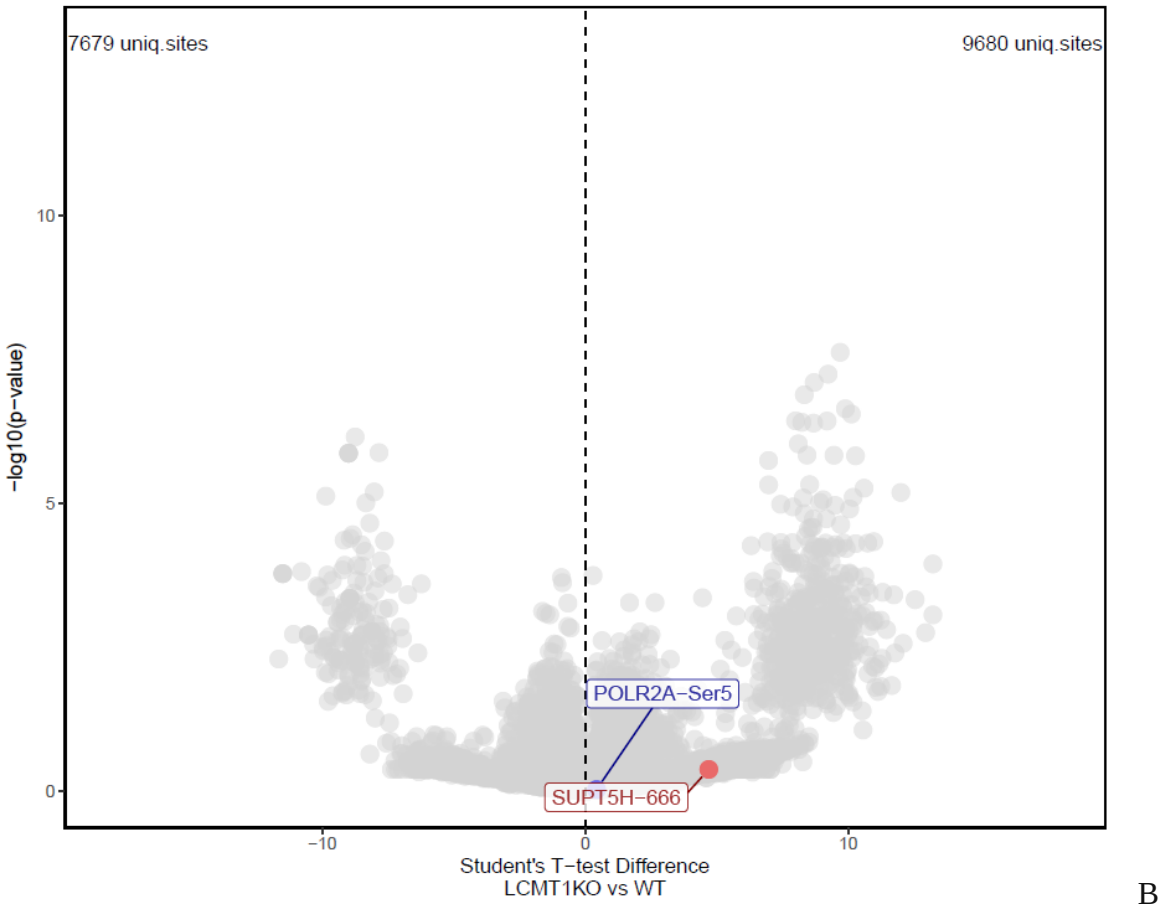

B

Figure 7. (A) The volcano plot above represents the TiO2 enrichment of 2 CTRL/LCMT1 KO replicates. On the right there are the unique peptide sites that are more phosphorylated in LCMT1 KO, on the left the ones more phosphorylated in CTRL. X axis = Student's T-test Difference of LCMT1 KO vs CTRL, Y axis = -$\log_{10}$(p-value). NELF-A and NELF-B are labeled in red, while NELF-E in blue. We can observe an increase of general NELF phosphorylation in LCMT1 KO sample. (B) Same figure but highlighting different residue and proteins: in blue RNA Polymerase II Serine 5, in red SPT5 Serine 666.

To assess the dynamic recruitment of PP2A to the chromatin in response to a LCMT1 short time depletion, ChIP-seq assays were performed using HeLa cells infected with shLUC and shLCMT1 lentiviruses and selected for 3 days. ChIP-seq assays were performed using antibodies specific for RNA Polymerase II, CTD Serine 2 phosphorylation (p-Ser2) and CTD Serine 5 phosphorylation (p-Ser5). Interestingly, sequencing data show that there is a decrease in RNA Polymerase II binding to the DNA in the sample depleted of LCMT1 (shLCMT1) (Fig. 8). The reduced binding

of RNAPII to DNA in the LCMT1-depleted sample indicates that LCMT1 plays a role in maintaining proper RNA Polymerase II recruitment to chromatin. This reduction in RNA Polymerase II binding may have implications for transcriptional activity.

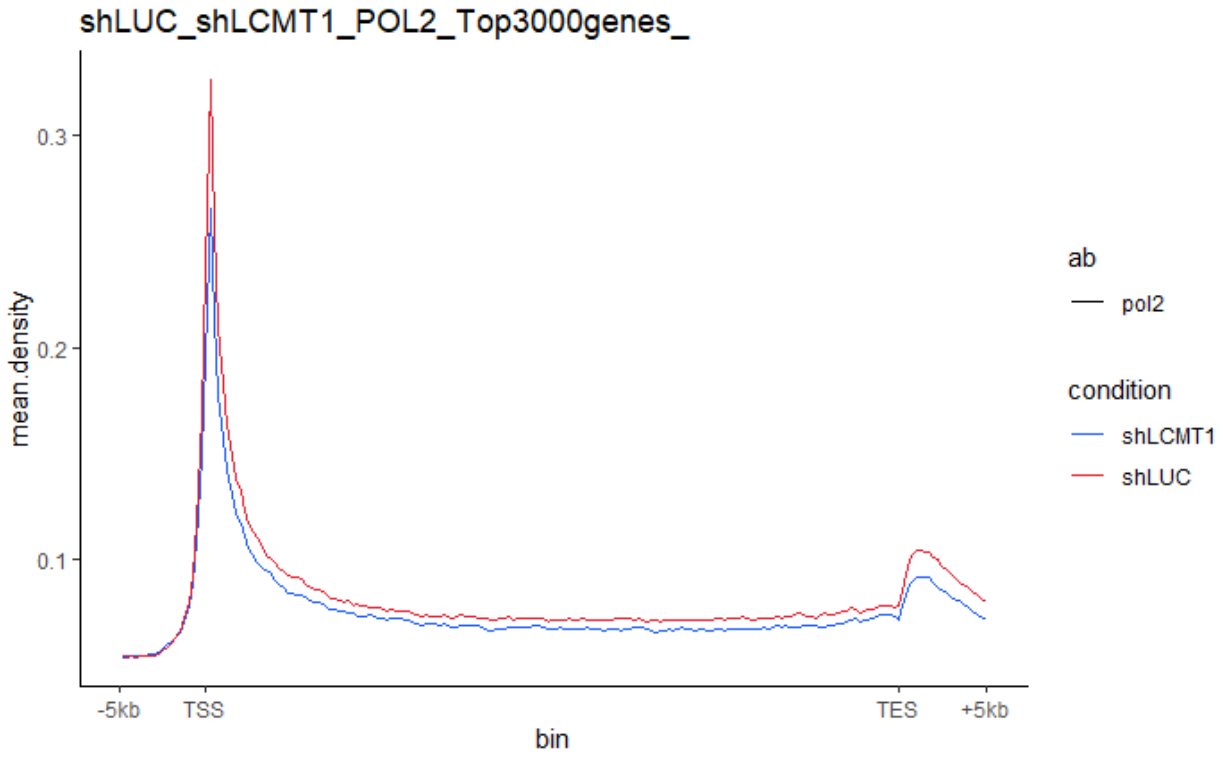

Figure 8. This graph represents the average profile of RNA Polymerase II in shLUC (red line) and shLCMT1 (blue line) HeLa. The genes considering are the top 3000 more expressed by RNA Polymerase II. At TSS (Transcription start site) RNA Polymerase II overgoes to pause hence it is possible to observe a very high peak. After Serine phosphorylation, it is released and start the productive elongation until it gets to the TES (Transcription end site). All samples overwent drosophila normalization. This graph shows that the amount of RNA Polymerase II at the start, gene body and termination is lower in cells with an increase of unmethylated PP2CA levels (shLCMT1).

LCMT1 knockdown (KD) in HeLa cells resulted in an increase in the phosphorylation of both Serine 2 and Serine 5 on RNA Polymerase II CTD (Fig. 8A – B). This finding is consistent with the hypothesis that methylated PP2A is the active form that can effectively dephosphorylate the CTD.

All p-Ser2 and p-Ser5 ChIP-seq data shown are normalized to total RNA Polymerase II levels.

In summary, in a cellular system depleted of LCMT1, PP2A is mostly unmethylated and less efficient to dephosphorylate RNA Polymerase II.

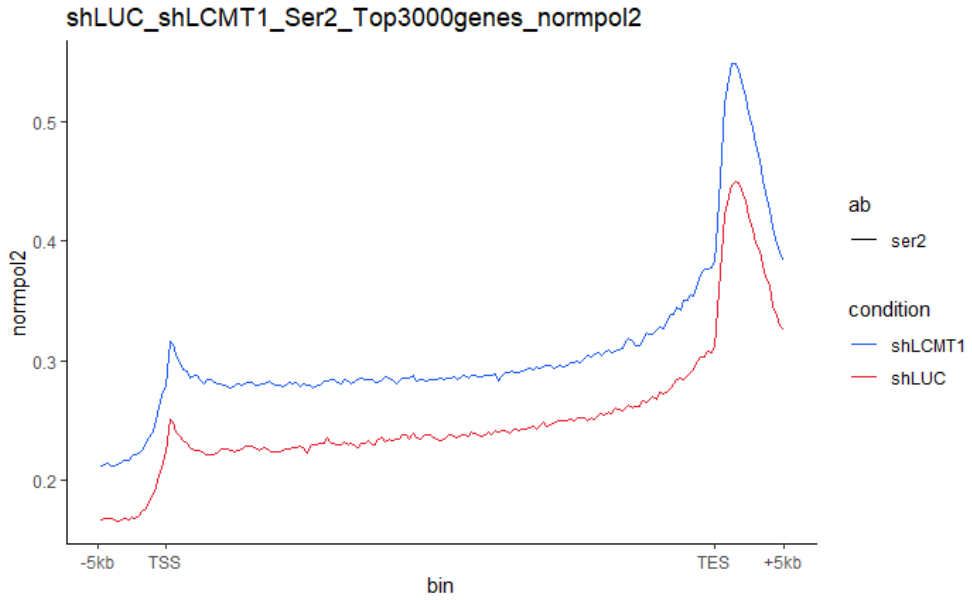

A

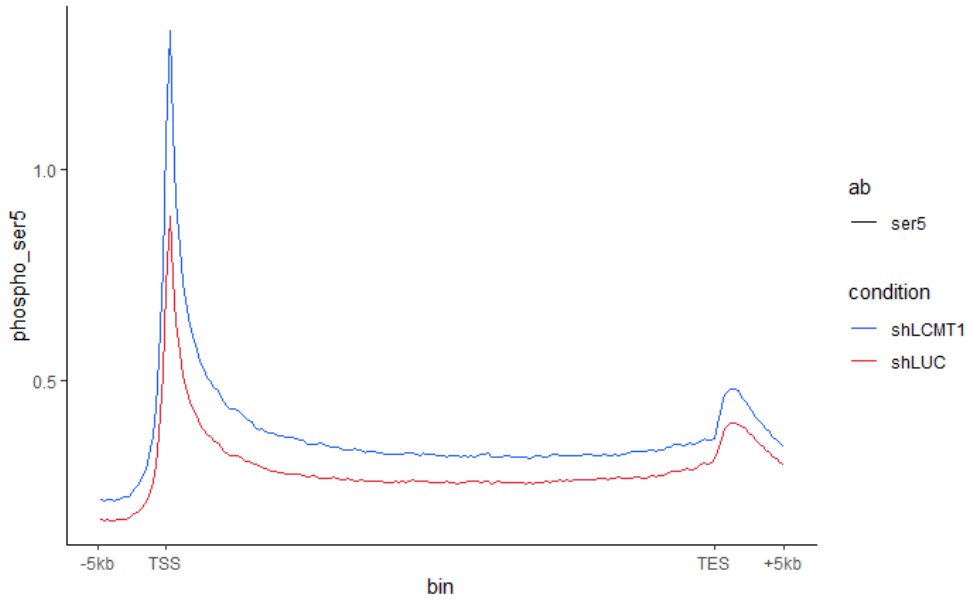

B

Figure 8. A and B graphs have to been read as the one shown above. shLUC (red line) and shLCMT1 (blue line). (A) represents the average profile of CTD Serine 2 (Ser2). The set of genes is the same to the one used for RNA Polymerase II average profile. At TSS, Serine 2 is barely phosphorylated, hence, the peak is very low. However, it is phosphorylated throughout the gene body and reaches the highest phosphorylation at the termination. Phosphorylated

Ser2 is more abundant in the sample with LCMT1 depletion. (B) represents the average profile of CTD Serine 5 (Ser5). Ser5 reaches the highest phosphorylation at the TSS. In the sample with higher unmethylated PP2A levels (shLCMT1) it is possible to observe an increase of Ser5 phosphorylation at TSS, gene body and TES. All samples overgoes drosophila normalization and are normalized to total RNA Polymerase II levels.

We decided to perform the same ChIP-seqs in WT/LCMT1 KO 293T cells. ChIP-seqs show an increase in RNA Polymerase II phosphorylation when methylated PP2CA levels decrease (Fig. 9A – B – C). The fact that these results were obtained in both HeLa and 293T cells suggests that the relationship between LCMT1 and PP2A methylation, and their effects on RNA Polymerase II phosphorylation, is not limited to a specific cell type. These findings provide deeper insights into the dynamics of transcriptional regulation and the critical role of PP2A methylation in this process.

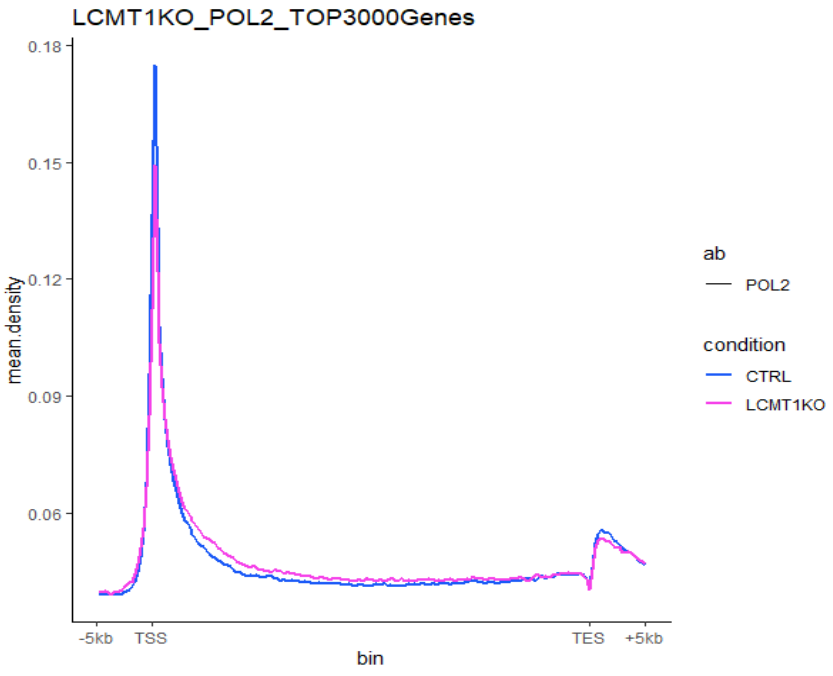

A

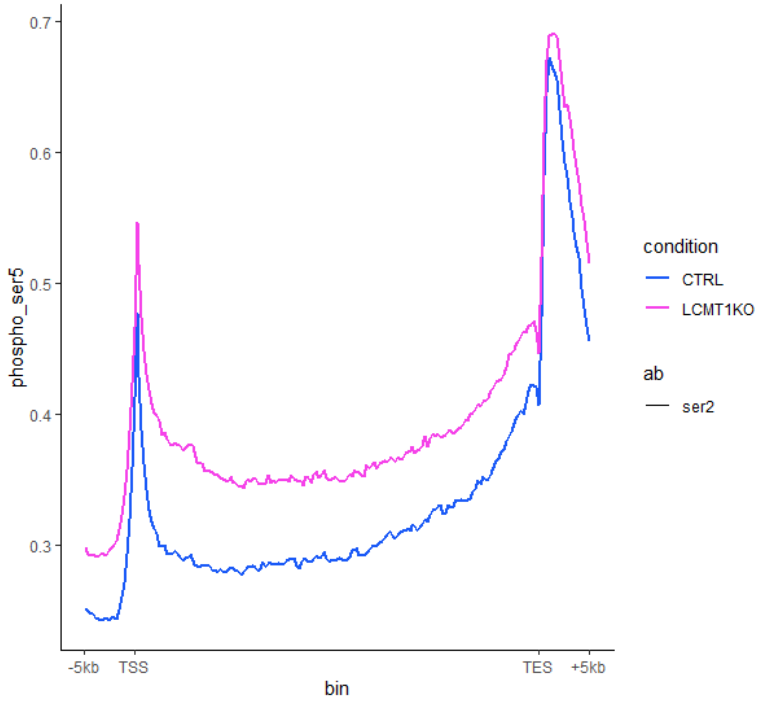

B

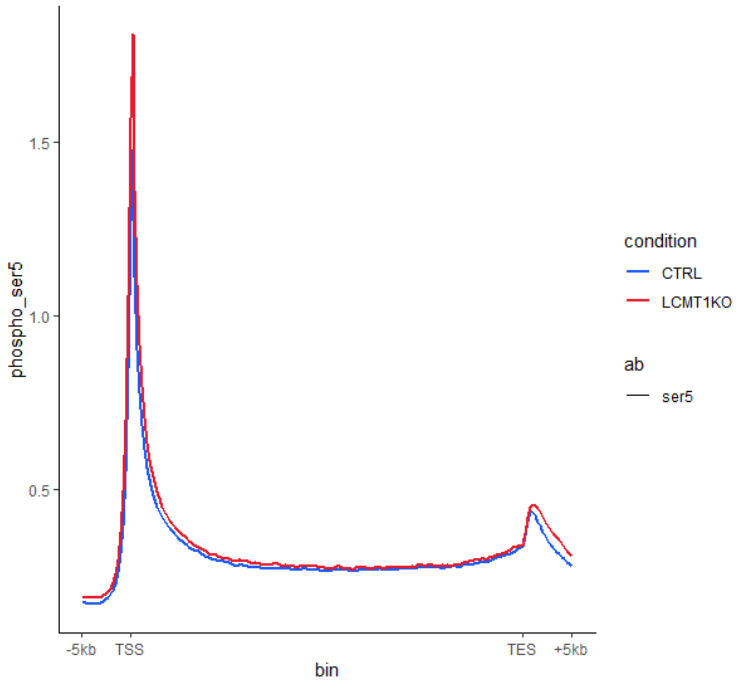

C

Figure 8. A, B and C represent the average profile of RNA Polymerase II, Ser2 and Ser5 in WT and LCMT1 KO 293T Cells. The genes taken in consideration are the top 3000 RNA Polymerase II most expressed. CTRL (WT) is in blue, LCMT1 KO in pink. RNA Polymerase II abundancy is higher in WT HeLa, on the contrary, Ser2 and Ser5

phosphorylation is increased in the sample lacking LCMT1. All samples undergo drosophila normalization. Ser2 and Ser5 are normalized to total RNA Polymerase II levels.

Our investigation into the RNA Polymerase II travel ratio, specifically the ratio between RNA Polymerase II coverage at the transcriptional start site (TSS) and the coverage at the gene body, is an important metric for understanding the dynamics of transcriptional regulation. Our finding that the depletion of LCMT1 does not significantly affect RNA Polymerase II travel on the DNA is a significant result. The RNA Polymerase II travel ratio reflects the balance between promoter-proximal initiation and transcriptional elongation. A stable travel ratio suggests that the initiation and elongation phases of transcription are not strongly impacted by LCMT1 depletion. These results highlight that while LCMT1 may influence specific aspects of transcription, such as CTD phosphorylation, it may not have a dramatic effect on overall RNA Polymerase II travel on DNA (Fig. 9 A – B).

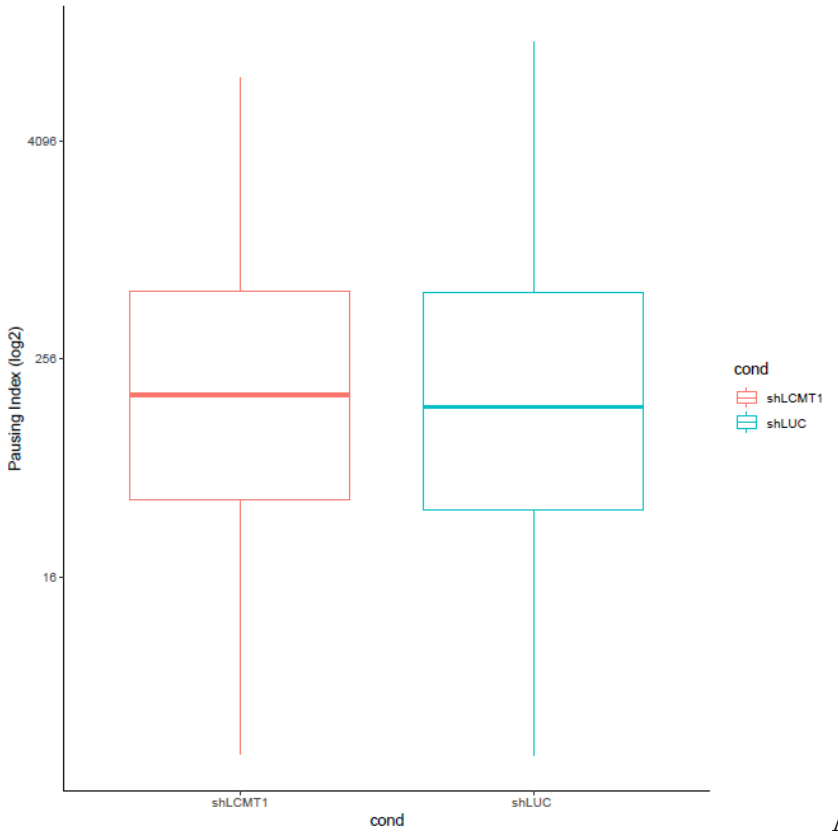

A

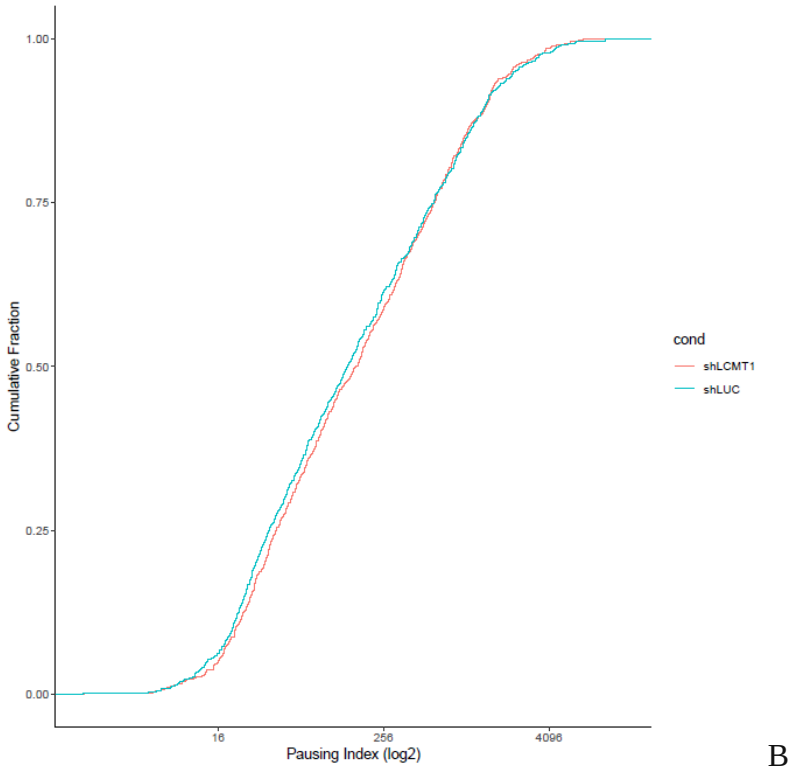

B

Figure 9. A and B pictures show the boxplot and the traveling curve of the RNA Polymerase II traveling ratio. shLUC is shown in light blue, shLCMT1 in orange. Both plots show there is not difference between the traveling ratio of shLUC and shLCMT1 RNA Polymerase II.

Increase of nascent RNA after LCMT1 level decrease

In transcription, the changes of RNA Polymerase II CTD phosphorylation affect RNA production. Since we observed an RNA Polymerase II hyper phosphorylation in cells depleted of LCMT1, we wanted to investigate if we can even see an increase in RNA transcription. To examine the impact of LCMT1 on RNA transcription, we performed Click-IT EU labeling and FastGRO experiments in HeLa cells, using Flavopiridol as a control (in Click-IT EU labeling assay).

HeLa cells were infected in 6 wells with shLUC and shLCMT1 lentiviruses and selected for 3 days. One shLUC well was treated with Flavopiridol and used as negative control. Flavopiridol, a CDK inhibitor, is a drug able to block transcription. 5-Ethinyl-uridine (EU) was added for 40 min before collecting cells. 1/3 of harvested cells was used to check the quality of LCMT1 depletion, 2/3 was used to perform the Click-IT experiments. Flow cytometry data show an interesting

increase in nascent RNA upon LCMT1 depletion which is in line with the earlier findings of RNA Polymerase II hyperphosphorylation when unmethylated PP2A levels increase (Fig. 10).

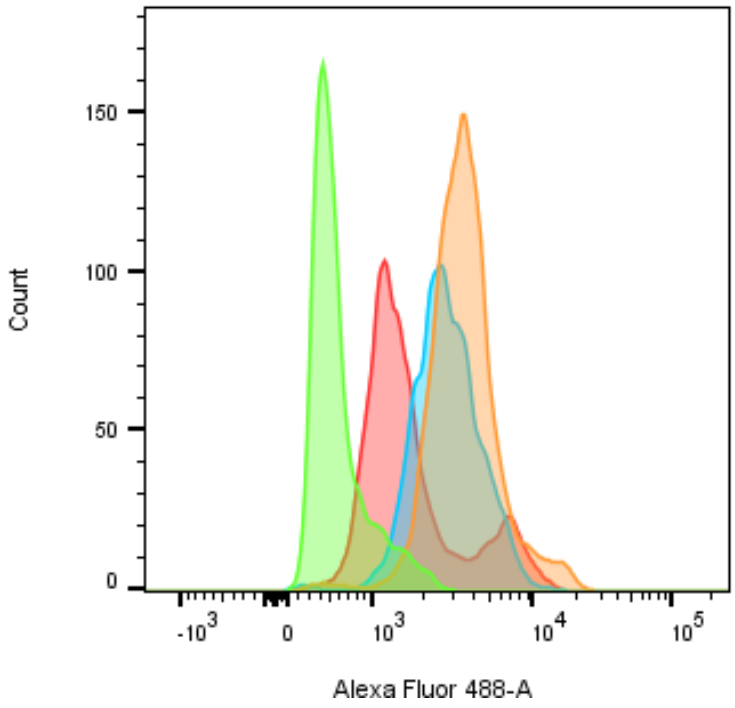

Figure 10. ClickIT of shLUC and shLCMT1 HeLa samples. Orange: shLCMT1 1, Blue: shLCMT1 2, Red: shLUC, Green: shLUC + Flavopiridol. Increase of nascent RNA upon LCMT1 decrease.

After investigating LCMT1 decrease role in nascent RNA, we asked how an LCMT1 increase could affect nascent RNA transcription. To assess that, we decided to use cells with an overexpressed LCMT1. We transfected HeLa cells with pLKO-HF-LCMT1- virus and confirmed the effectiveness of LCMT1 overexpression by WB (FLAG and HA antibodies were used) (Fig. 11).

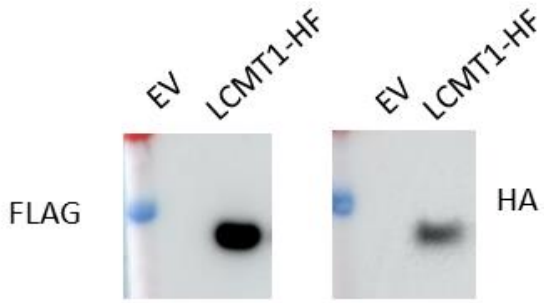

Figure 11. The WB shown above represents the over-expression of HF-LCMT1 in HeLa cells after 2 days. Membranes were incubated with FLAG and HA antibodies.

ClickIT assay was performed in LCMT1 over-expressed HeLa and visualized by flow cytometry. Interestingly, data show that decrease of nascent RNA is subsequent to LCMT1 level increase (increase of unmethylated PP2CA) (Fig. 12). By conducting experiments to both deplete and overexpress LCMT1, we created a comprehensive understanding of LCMT1 role in transcription regulation.

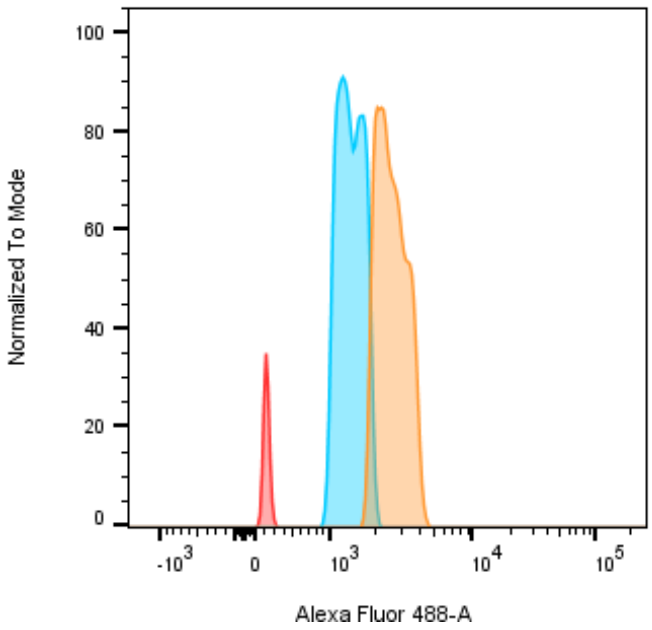

Figure 12. ClickIT of over-expressed LCMT1-HF. Empty vector (EV) is in orange, LCMT1-HF in blue and EV treated with flavopiridol in red. Notable decrease of nascent RNA when LCMT1 levels increase. Samples were normalized using the Modal option which scales all channels as a percentage of the maximum count. Flow cytometry data were analyzed with FlowJo.

To assess the importance of LCMT1 catalytic site and its specificity in modulating RNA transcription, we decided to over-express a R73A (catalytic site) point-mutated HF-LCMT1 to investigate its function when WT LCMT1 is depleted. We performed the same Click-IT experiments described above after transfecting LCMT1-depleted HeLa with pLKO-HF-

LCMT1(R73A) plasmid. The fact that LCMT1 R73A is unable to perform the wild-type LCMT1 activity and that the flow cytometry experiment still shows an increase in nascent RNA transcription when LCMT1 is depleted and the mutant LCMT1 is expressed (Fig. 12), demonstrated that the catalytic function of LCMT1 is necessary for its regulatory role in nascent RNA process and that other factors cannot compensate for this specific function.

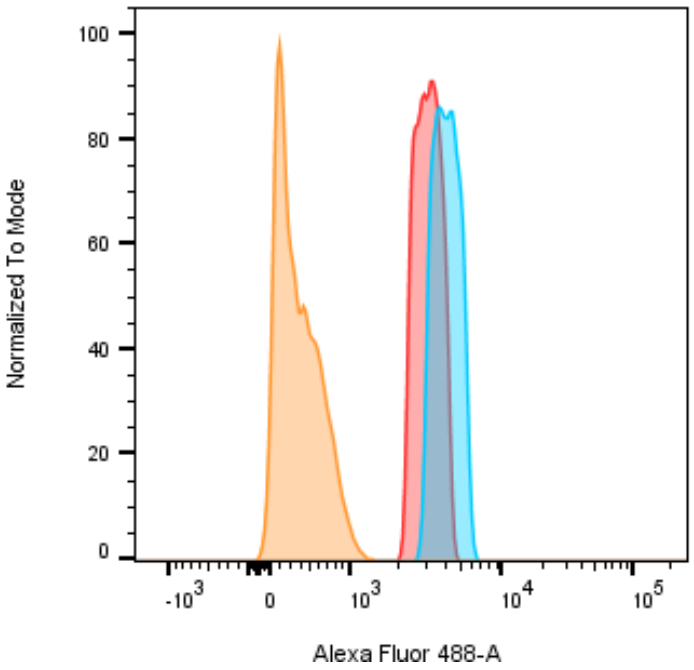

Figure 12. ClickIT of over-expressed HF-LCMT1(R73A). Empty vector (EV) is in red, HF-LCMT1(R73A) in blue and EV treated with flavopiridol in orange. Notable increase of nascent RNA when WT LCMT1 is depleted and point mutated LCMT1 is overexpressed. Samples were normalized using the Modal option which scales all channels as a percentage of the maximum count. Flow cytometry data were analyzed with FlowJo.

We performed the same assay in LCMT1 KO 293T Cells. They underwent the same treatment with Flavopiridol and EU. The Click-IT assay was executed as described before. The consistency of our results, showing an increase in nascent RNA in LCMT1 KO cells, further reinforces the role of LCMT1 in transcriptional regulation (Fig. 13). The consistent observation of increased nascent RNA in LCMT1-depleted cells, whether through long-term or short-term depletion, supports the reliability and reproducibility of our results.

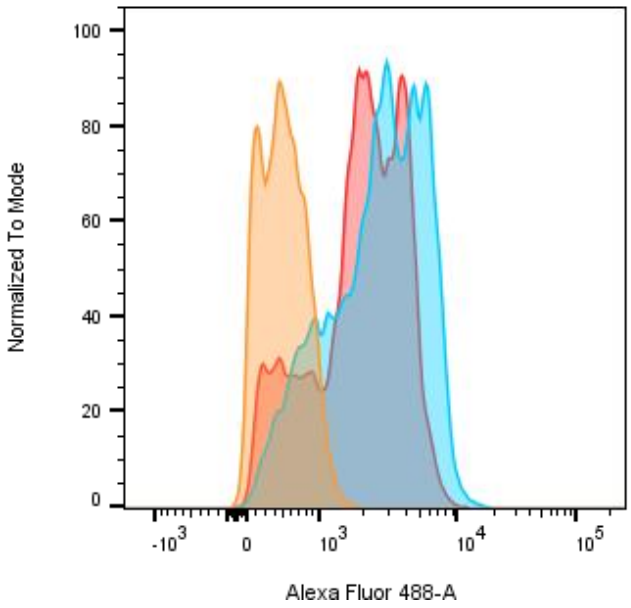

Figure 13. This plot represents the incorporation of EU in nascent RNA in WT and LCMT1 KO 293T. CTRL/WT is in red, LCMT1 KO in blue. An increase of nascent RNA production (shift on the right) occurs in the sample lacking LCMT1. The orange sample is the treatment with flavopiridol. Here nascent RNA levels are brought down since transcription is blocked. Samples were normalized using the Modal option which scales all channels as a percentage of the maximum count. Flow cytometry data were analyzed with FlowJo.

The second approach we decided to use to analyze nascent RNA profile was via fastGRO that was developed in the Gardini lab. This technique requires nuclei isolation and labeling of nascent RNA with a solution containing 4-thio-UTP. RNA is isolated by TRIzol and then fragmented. 4-thio-UTP-containing RNA is biotinylated with biotin-HPDP and recovered by IP with streptavidin beads. Labeled RNA is eluted in DTT and used for NGS library preparation (Barbieri et al., 2020).

shLUC and shLCMT1 infected HeLa cells were selected for 3 days before collecting them. All samples were added drosophila nuclei for normalization. The use of seqMINER for cluster analysis and gene selection from the 3000 most expressed genes by RNA Polymerase II, followed by deeper analysis using deeptools, enhances the robustness of our findings.

The key result, which confirms our flow cytometry findings, is the notable increase in nascent RNA in the cellular system where PP2CA is mostly unmethylated (Fig. 14). This strengthens the validity of our findings and underscores the role of PP2A methylation in regulating nascent RNA synthesis.

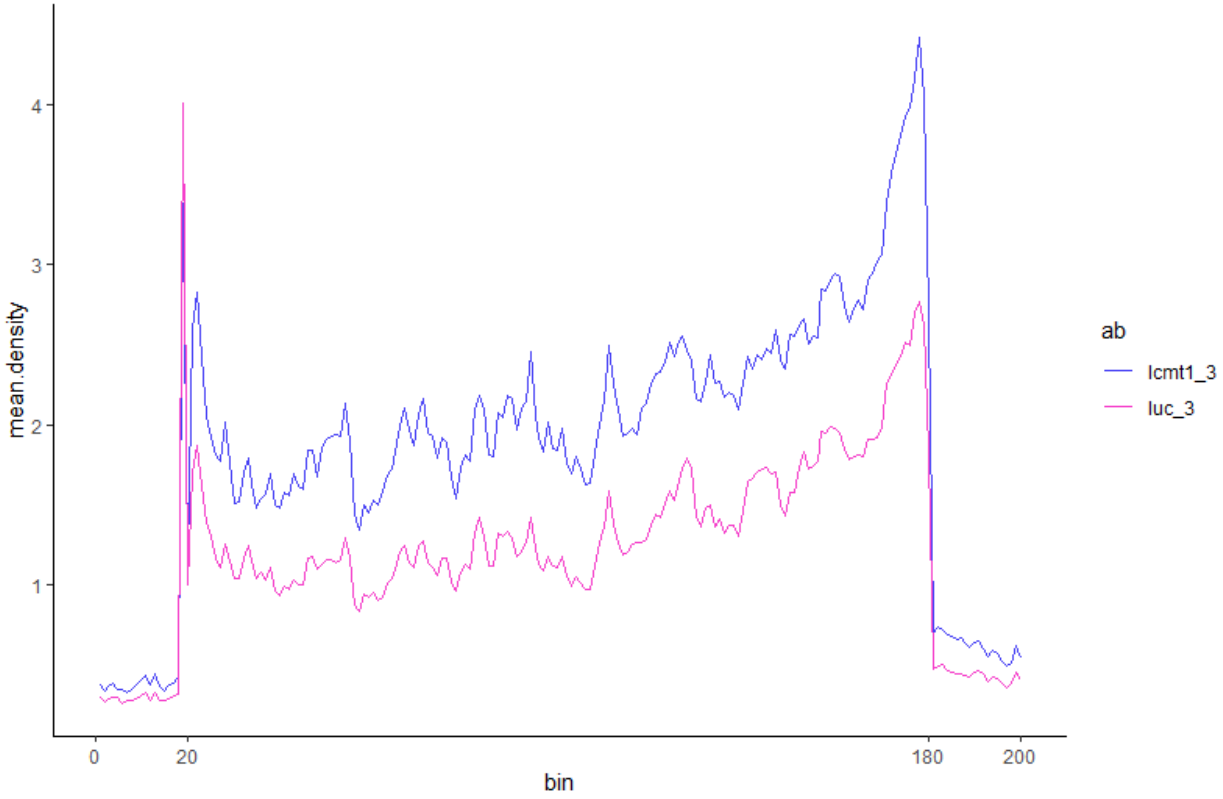

Figure 14. The picture above represents the average profile of 3000 most expressed genes by RNA Polymerase II of nascent RNA. The third replicate is shown here. In blue: shLCMT1, in pink: shLUC. There is an increase in nascent RNA upon LCMT1 KD. Samples have been normalized with Drosophila.

The combination of flow cytometry data and fastGRO analysis offers a comprehensive understanding of how LCMT1 affects nascent RNA production.

Decrease of steady-state RNA after LCMT1 level decrease

To further investigate broader affects in transcription and RNA production by LCMT1, after analyzing nascent RNA, we moved our interest to the steady-state RNA. To assess that, we

collected HeLa cells infected with shLUC and shLCMT1 viruses and selected for 3 days for Total RNA-seq. Data obtained from Illumina sequencing were analyzed with DeSEQ2. PCA plot shows that sample classification was appropriate, reinforcing the reliability of the data (Fig. 15 A).

The most striking result is the unexpected decrease in gene expression upon LCMT1 depletion (Fig. 15 B). This contradicts the earlier findings of increased nascent RNA and the hyperphosphorylation of RNA Polymerase II after LCMT1 depletion. It indicates that LCMT1 role in transcription regulation is complex and may have both positive and negative regulatory functions.

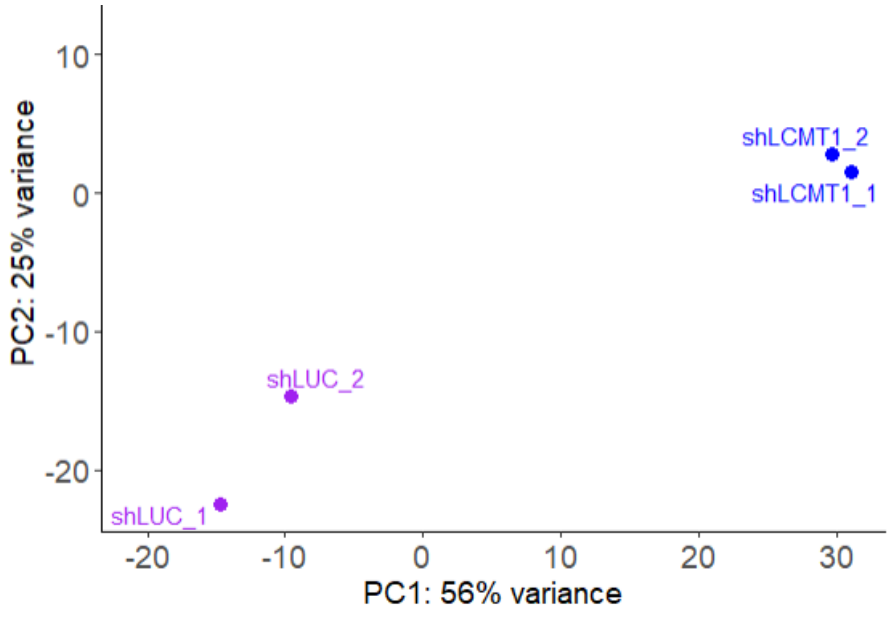

A

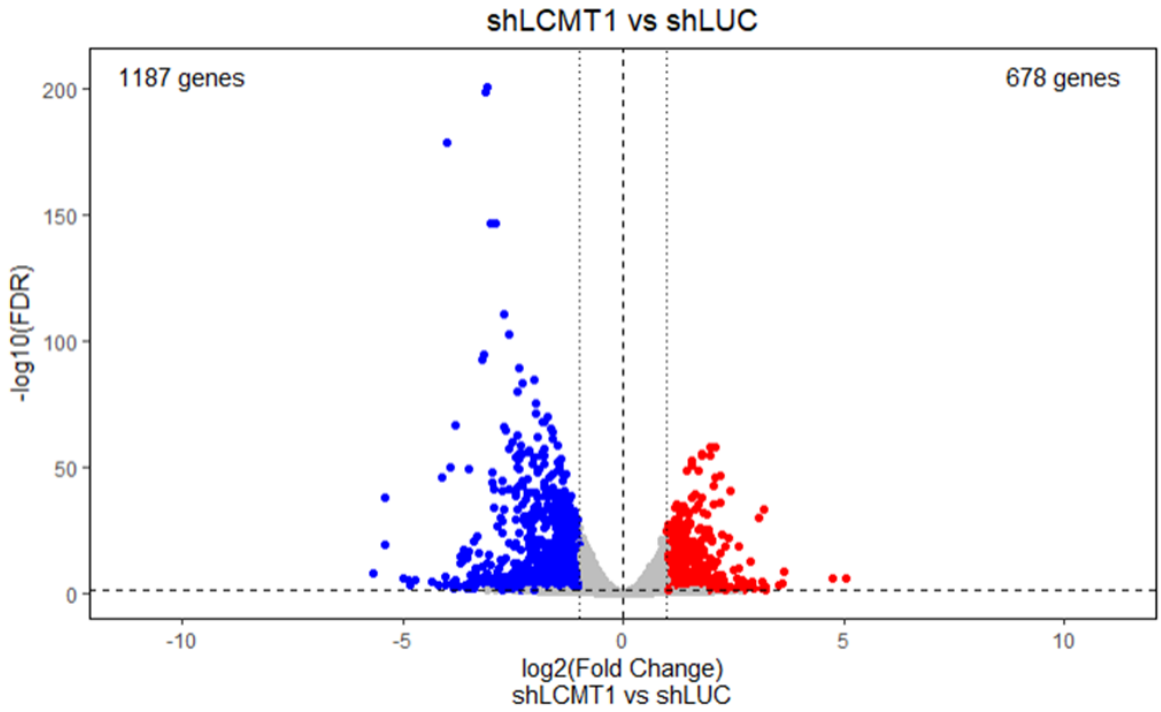

B

Figure 15. Figure A shows PCA. All replicates cluster together. Figure B represents volcano plots of total RNA-seq of LCMT1. ShLCMT1 volcano plot shows a decrease of gene expression in LCMT1-depleted sample.

IPA (Ingenuity Pathway Analysis) does not seem to be very informative. There is not any interesting pathway to be highlighted.

The discrepancy between our results on nascent RNA and steady-state RNA, where nascent RNA levels increased while steady-state RNA levels decreased upon LCMT1 depletion, suggests that LCMT1 may indeed have a role in post-transcriptional processes, such as transcription termination or splicing defects, which can impact RNA stability. This interpretation aligns with the observed data and highlights the complexity of LCMT1 role in gene expression regulation. To gain a deeper understanding of LCMT1 specific roles in transcription and post-transcriptional regulation, further experiments and analyses focused on termination, splicing, and RNA stability would be beneficial.

Unmethylated PP2CA binds more splicing proteins than methylated PP2CA

Our findings suggest a potential link between PP2A methylation status and RNA maturation processes, such as RNA cleavage, splicing, etc. Even though we have not been able to perform the transcriptomic experiments and analysis yet, the proteomic data provides some valuable insights. The mass spectrometry data from PP2CA 1D6 immunoprecipitation in both the shLUC and shLCMT1 nuclear extracts shows an increase in splicing/RNA cleavage protein binding to PP2CA in the sample lacking LCMT1 (more unmethylated PP2CA) (Fig. 16). This suggests a direct correlation between PP2A methylation status and RNA maturation protein binding. Even if the significance of this increase is not substantial, it may still indicate a functional connection between PP2A methylation and splicing. The fact that we observe similar results in two different experimental setups, comparing WT and LCMT1 KO nuclear extracts as well, helps the reliability of our findings. This consistency strengthens the argument that unmethylated PP2A is associated with stronger splicing protein binding. For now, our first goal is to answer this question: How might altered PP2A methylation affect the splicing/RNA maturation process? The lack of transcriptomic data, actually, restricts our ability to draw more precise conclusions about how these methylation status changes might affect splicing. We are planning, hence, to perform an RNA long-read sequencing with nanopore, which will allow us to gain a more detailed and comprehensive understanding of splicing events in the context of PP2A methylation. With longer reads, we can directly observe splice junctions and identify different isoforms of genes. This will allow us to quantify and characterize splicing events that shorter reads might miss.

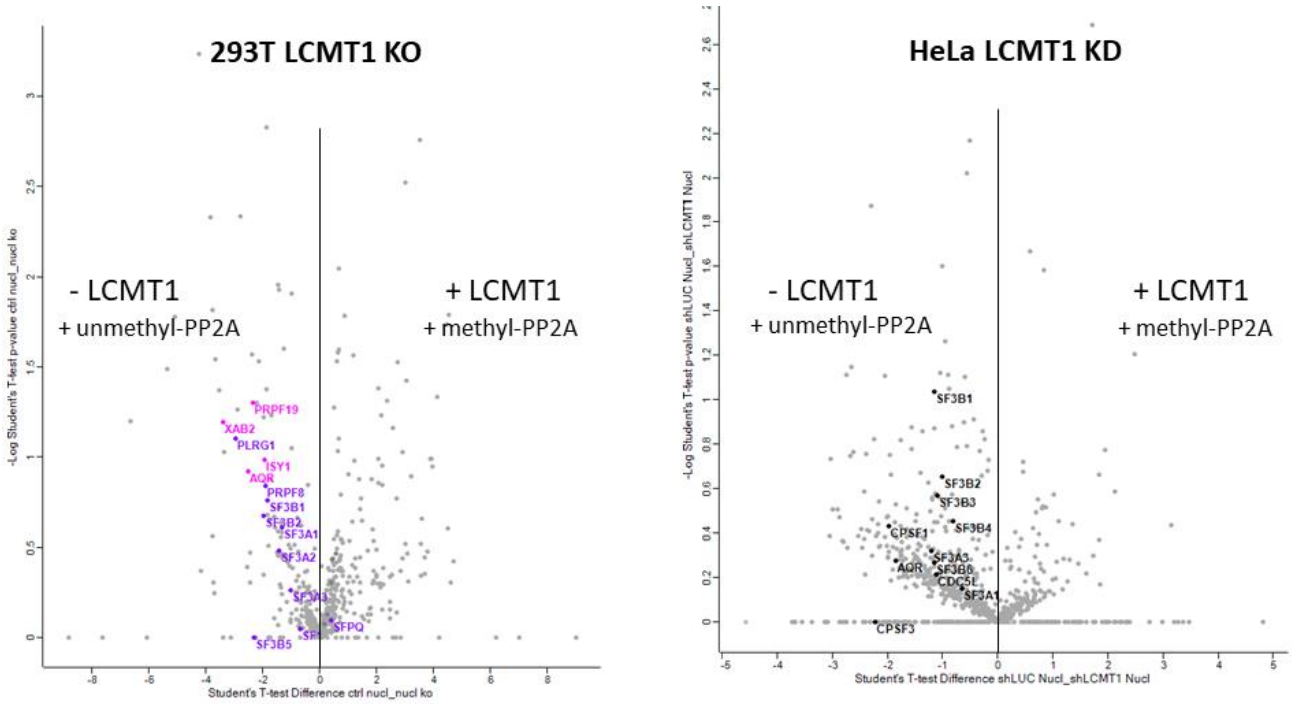

Figure 16. The two plots above show the splicing protein binding to PP2CA both in a WT and in a LCMT1-depleted system. The plot on the left is WT/LCMT1 KO PP2CA IP, the plot on the right is shLUC/shLCMT1 PP2CA IP. The left side of each plot represents the LCMT1 KO/LCMT1 KD condition, the right one WT/shLUC condition. Almost all proteins involved in RNA maturation (splicing or cleavage and polyadenylation) are visibly binding unmethylated PP2CA. All samples have been normalized to total PP2A levels. Data were analyzed with Perseus.

PP2A-INT complex binds mostly splicing proteins

We decided to perform a TURBOID assay (Targeted Ubiquitin Ligase-Related BioID) to further investigate the potential interaction between PP2A and proteins involved in RNA maturation. TurboID-based proximity labeling assay is a strategy that allows the detection of in vivo protein-protein interactions (far each other not more than 10-15 nm) using a biotin-ligase enzyme that adds biotin groups to proteins in close proximity (Fig. 17).

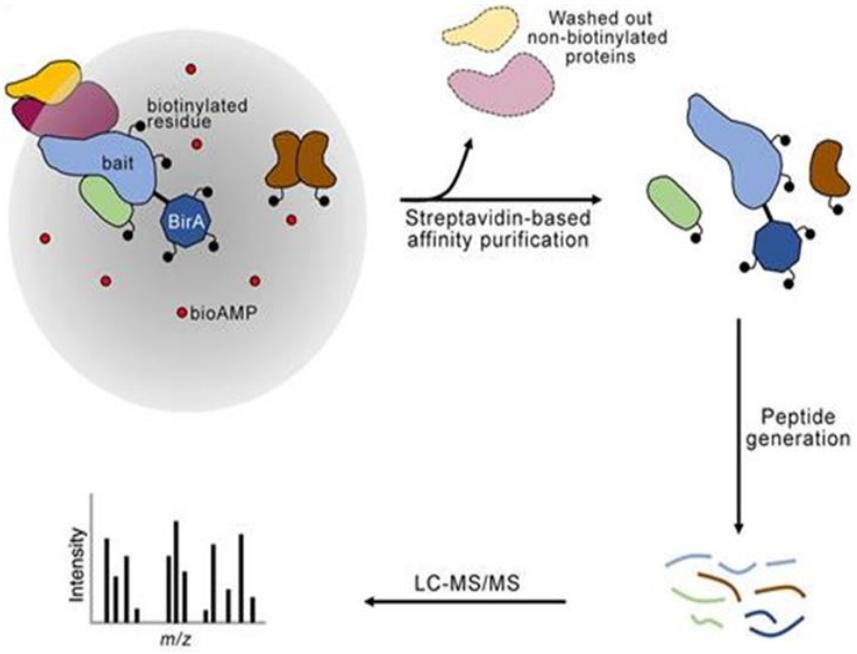

Fig 17. *Kelvin F. Cho, et al., 2020*

Since we saw that in the nucleus, PP2A is mostly bound to Integrator, we decided to attach the TurboID sequence to INTS6 rather than PP2A because we thought that looking at all PP2A interactions would have been complex and challenging to interpret. To do that, first, we designed our plasmid of interest: we cloned TurboID sequence into pINTO-INTS6-HF (made by one of my colleagues) (Fig. 18).

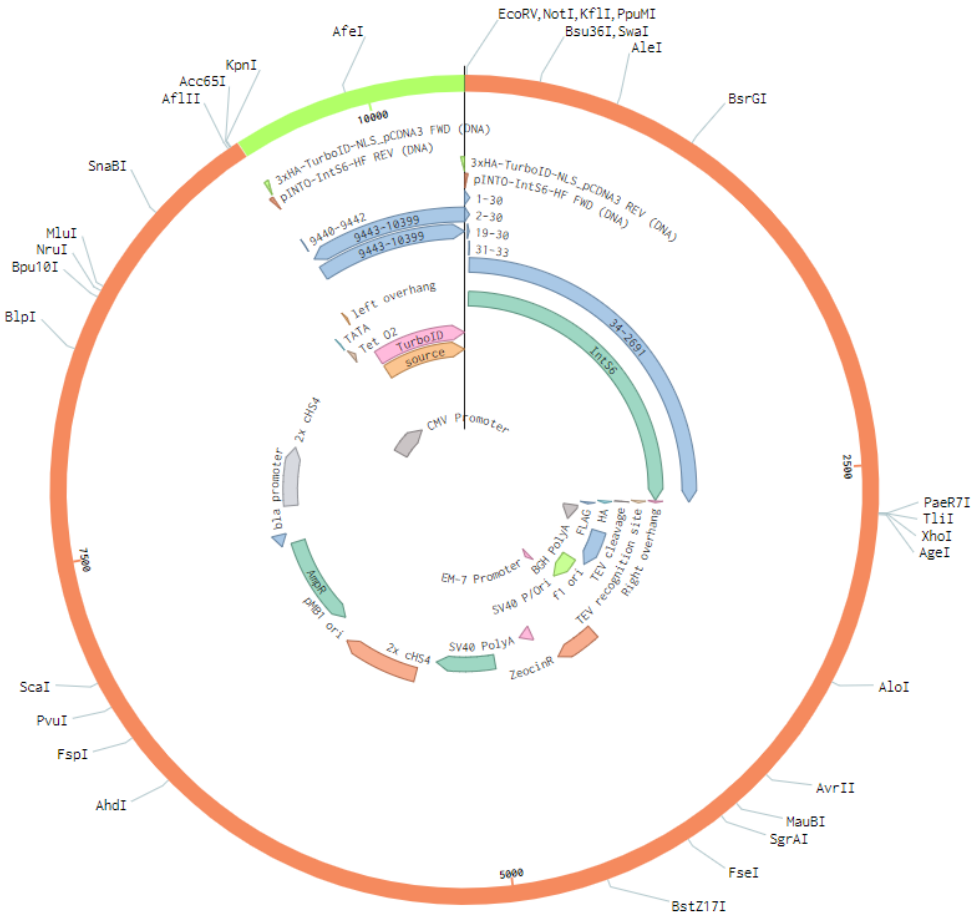

Figure 18. The picture above shows the map of the cloned plasmid used to perform TurboID assay: pINTO-TurboID-INTS6-HF.

We transfected 293T cells both with pINTO-TurboID-INTS6-HF and pINTO-INTS6-HF (it represents the negative control). Cells were treated with Biotin for 10 min and then collected and lysed. The increase of biotinylation was checked with Streptavidin-HR antibody (Fig. 19).

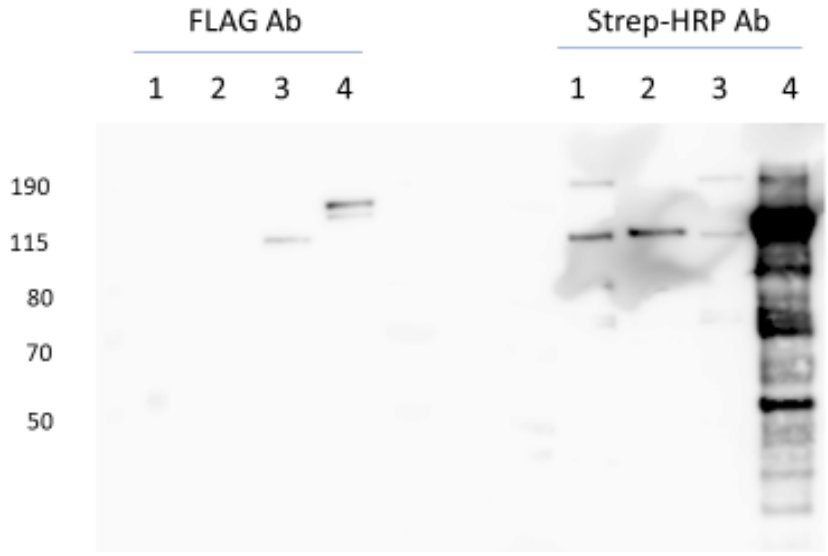

Figure 19. The WB shown above represents both pINTO-INTS6-HF and pINTO-TurboID-INTS6-HF transfection and the efficiency of biotinylation after adding biotin for 10 min. Sample numbers are: 1) 293T WT total cell lysate, 2) 293T WT + 50 uM biotin total cell lysate, 3) 293T transfected with pINTO-INTS6-HF + 50 uM biotin total cell lysate, 4) 293T transfected with pINTO-TurboID-INTS6-HF + 50 uM biotin total cell lysate. The WB on the left is blotted with FLAG ab and shows the transfection efficiency. The WB on the right is blotted with Streptavidin-HRP ab and shows the biotinylation increase after transfecting 293T with pINTO-TurboID-INTS6-HF and adding biotin. Samples #3 and #4 have been treated same way (same transfection and biotinylation conditions) but transfected with different plasmids. It is possible to observe that the presence of TurboID determines the increase of biotinylation in cells in only 10 minutes.

The assay was performed incubating the whole cell lysate with magnetic streptavidin beads for 1h at RT and overnight at 4 ˚C rotating. The eluate was used both for WB (to see if we got a biotinylation enrichment) and for MS (Fig. 20).

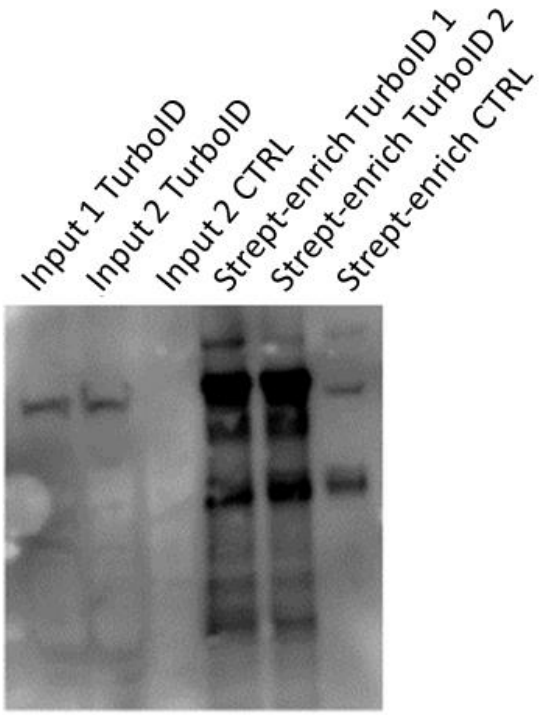

Figure 20. The WB shown above represents the biotinylation enrichment after TurboID assay. TurboID = cells transfected with pINTO-TurboID-INTS6-HF; CTRL = cells transfected with pINTO-INTS6-HF. We can observe a streptavidin enrichment in samples transfected with TurboID plasmid.

4 replicates have been performed and data were analyzed with Perseus software from which we were able to get Fold change of the sample enriched with streptavidin (cells transfected with pINTO-TurboID-INTS6-HF) over the sample transfected with pINTO-INTS6-HF (no streptavidin enrichment occurred) and the p-value. The identification of proteins from the XAB2 complex, PRPF19, AQR, CDC5L, SNRNP200, and the SF3 family, is a remarkable finding. This indicates that INTS6-PP2A might play a role in splicing events dephosphorylating some substrates important for splicing events (Fig. 21 A - B). The fact that many of the proteins identified through TURBOID have not been observed in other immunoprecipitation data suggests that the TURBOID approach can reveal distinct protein interactions. Moreover, TURBOID pulls down many DNA damage proteins, which is something we expect considering the connection between INTS6 and INTS3, that is involved in DNA repair processes. As we expect, in the TURBOID-INTS6 MS we also find all INT subunits and most of the proteins related to transcription.

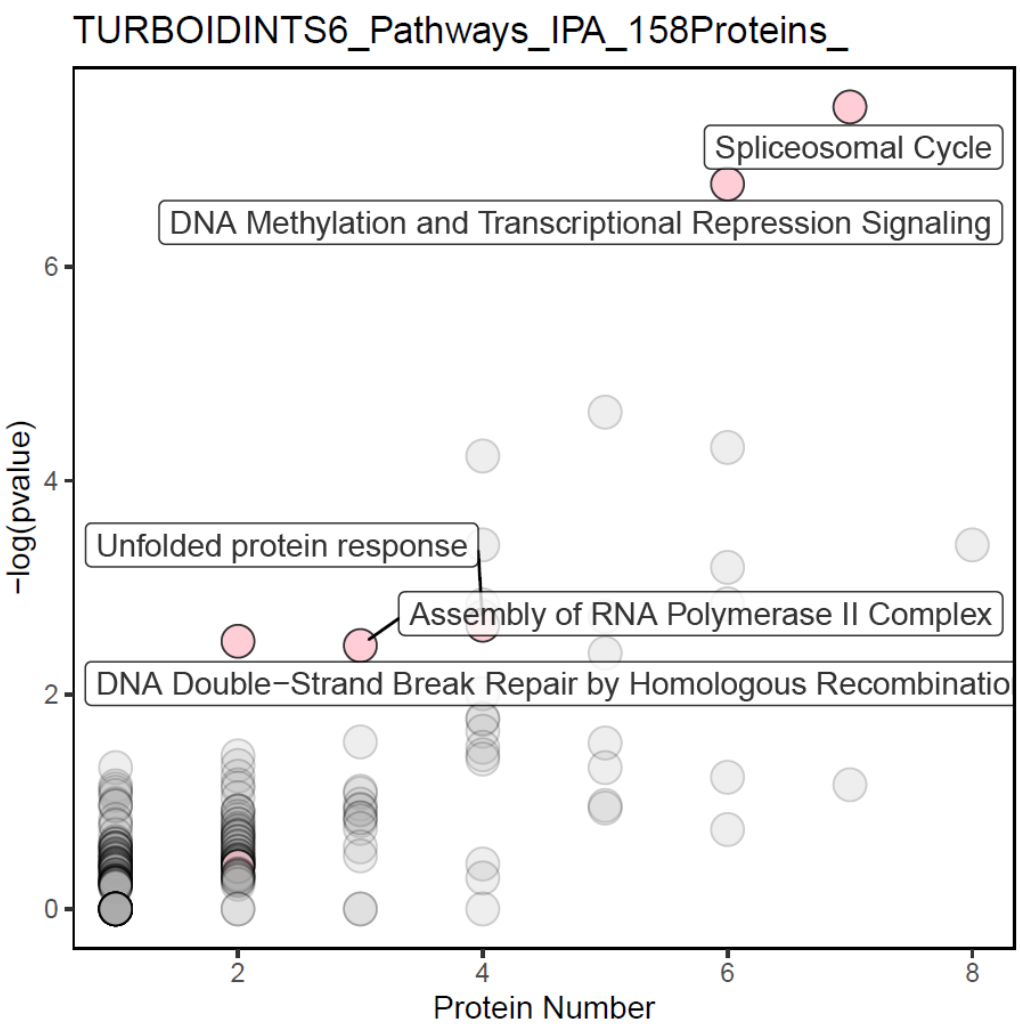
TURBOIDINTS6_Pathways_IPA_158Proteins_
Spliceosomal Cycle
DNA Methylation and Transcriptional Repression Signaling
Unfolded protein response
Assembly of RNA Polymerase II Complex
DNA Double−Strand Break Repair by Homologous Recombinatio
−log(pvalue)
0
2
4
6
2
4
6
8
Protein Number

A

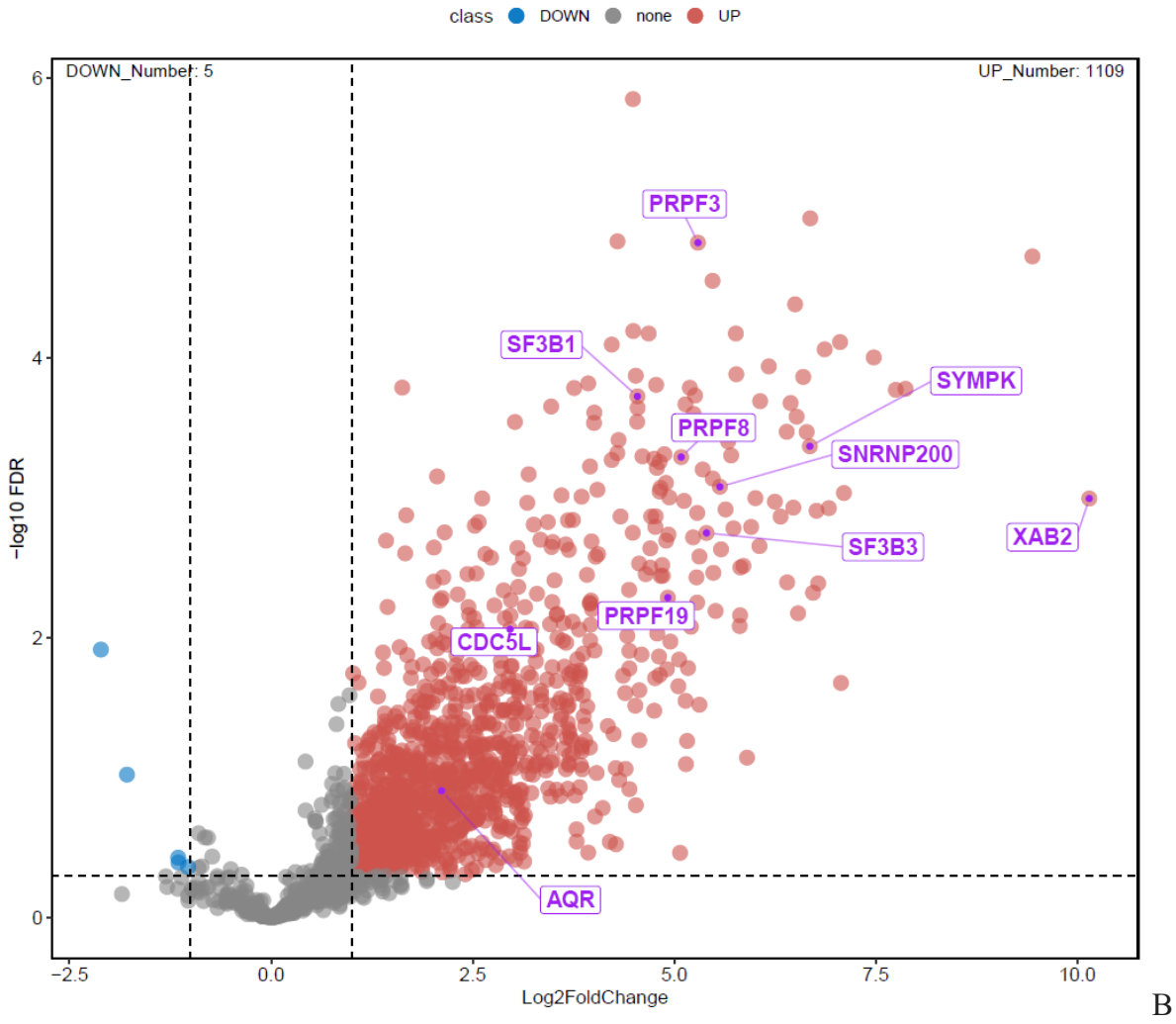

Figure 21. The picture (A) represents the Ingenuity Pathway Analysis (IPA) of 158 proteins with higher -log(p-value). Splicing cluster is the one with the highest kjnumber of proteins and -log(p-value). (B) This plot represents MS data obtained from TurboID-INTS6 assay. X axis = log2 fold change of pINTO-TurboID-INTS6-HF over pINTO-INTS6-HF; y axis = -log p-value. In purple, the main splicing proteins were labeled. There are 1109 significant proteins in TurboID experiment.

The identification of SMARCAD1 as a protein that binds to INTS6 in our TURBOID assay, despite not being observed in other immunoprecipitation experiments, is a noteworthy finding. SMARCAD1 role as a chromatin regulator is intriguing, and it is interesting to consider its potential involvement in splicing, even if it is not a focus of my thesis. This discovery may have

broader implications and opens up possibilities for future research directions beyond my current project.

To validate the results we obtained, we thought to perform the same TURBOID assay and experiments described above using the construct pINTO-TURBOID-INTS3-HF and pINTO-INTS3-HF (as control). The fact that we observed the same results with the pINTO-TURBOID-INTS6-HF construct as with the pINTO-TURBOID-INTS3-HF construct reinforces the idea that PP2A-INT plays critical roles in splicing and RNA maturation probably by dephosphorylating some of these substrates (Fig. 22). The link between the phosphorylation status of some of these substrates (we saw that in phosphoproteomics analysis) and the methylation status of PP2A is an intriguing discovery that can shed light on the regulatory mechanisms of splicing and RNA maturation by PP2A.

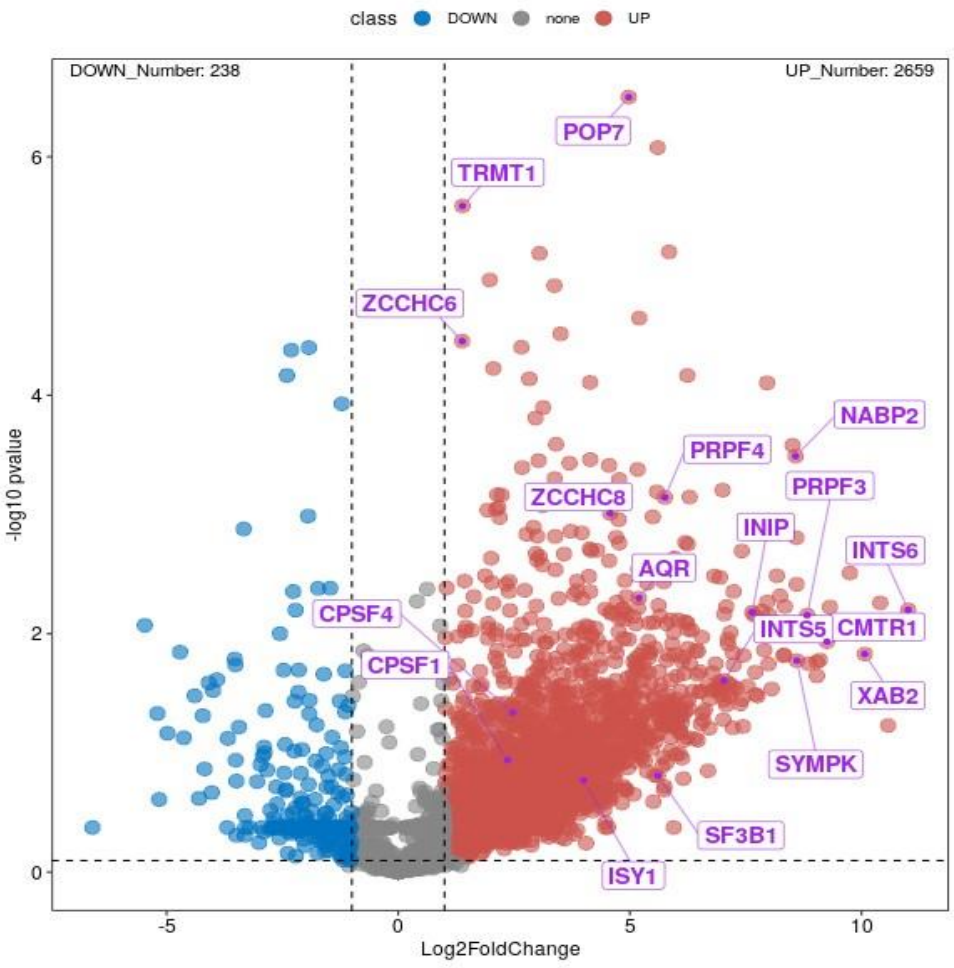

Figure 22. This plot represents MS data obtained from TurboID-INTS3 assay. X axis = log2 fold change of pINTO-TurboID-INTS3-HF over pINTO-INTS6-HF; y axis = -log p-value. In purple, the main splicing proteins were labeled. There are 1109 significant proteins in TurboID experiment.

LCMT1 localizes mostly in cytoplasm, PPME1 in both nucleus and cytoplasm

Our western blot analysis of the nuclear and cytoplasmic fractions from WT HeLa cells provides important insights into the subcellular localization of LCMT1 and PPME1. These results are crucial in understanding the context of PP2A methylation and its role in transcriptional regulation. The western blot results confirm that LCMT1 is predominantly located in the cytoplasm, which aligns with the existing literature. This localization reinforces its role in the cytoplasmic regulation of PP2A. Despite LCMT1 being primarily cytoplasmic, our data show that methylated PP2A is still the active form capable of dephosphorylating RNA Polymerase II and other transcription factors, which suggests that methylation status is maintained or influenced in both the nucleus and cytoplasm. PPME1 data do not align with the existing literature, which affirms that PPME1 is mainly nuclear. Our WB data suggests that PPME1 localization is as cytoplasmic as nuclear (Fig. 23).

WB was performed as follows: 6 and 12 ug of nuclear and cytoplasmic extracts from HeLa cells were loaded and membrane was incubated with LCMT1, PPME1 and GAPDH (ctrl) antibodies.

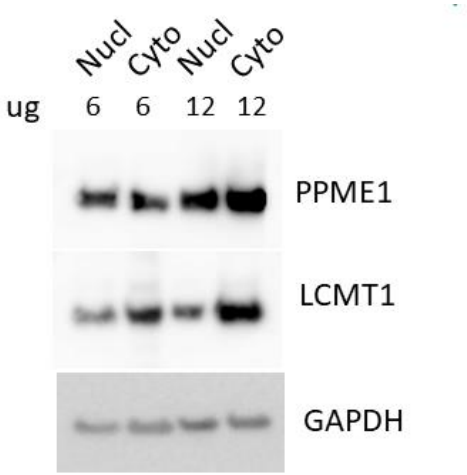

Figure 23. The WB above shows the expression of LCMT1 and PPME1 in nucleus and cytoplasm. 6 ug and 12 ug of each extract has been loaded. Membranes were incubated with PPME1, LCMT1 and GAPDH antibodies. LCMT1 is more expressed in cytoplasm, while PPME1 is expressed in both compartments.

Given the observed discrepancies in our Western blot data and literature, we thought to consider alternative techniques, such as immunofluorescence microscopy, to gain a more accurate and detailed understanding of PPME1 subcellular localization in our specific cell system (see the following paragraph).

PPME1 binds the chromatin and co-localizes with RNA Polymerase II

Previous experiments have shown that PP2A needs to be methylated to dephosphorylate RNA Polymerase II and certain transcription factors. This methylation state is essential for its activity in controlling the phosphorylation status of these proteins. Decreasing the levels of LCMT1, leads to an increase in the phosphorylation of CTD (C-terminal domain of RNA Polymerase II). Unmethylated PP2A is less unable to dephosphorylate its substrates, which allows CDK9 to freely phosphorylate them without checkpoint control. We are now considering the idea of inactivating PP2A by demethylating it, and we are wondering whether PPME1 plays a role in regulating PP2A during transcription. The research is shifting its focus to investigating the function of PPME1 in transcription regulation and its potential role in PP2A activation/inactivation. However, the data on PPME1 is currently inconclusive, but it is seen as a promising starting point for further research. To study the impact of PPME1 depletion on transcription, we performed some experiments using HeLa cells. Cells were infected with shLUC and shPPME1 and selected for three days. They were treated with Flavopiridol (a negative control) and 5-Ethynil-Uridine (EU) for 40 minutes to assess nascent RNA production. The decrease in PPME1 appears to result in a slight decrease in nascent RNA, which is the opposite of the effect seen after LCMT1 depletion (Fig. 24). This suggests that LCMT1 and PPME1 may have antagonistic roles in regulating PP2A, reinforcing the importance of PP2A methylation in early-stage transcription.

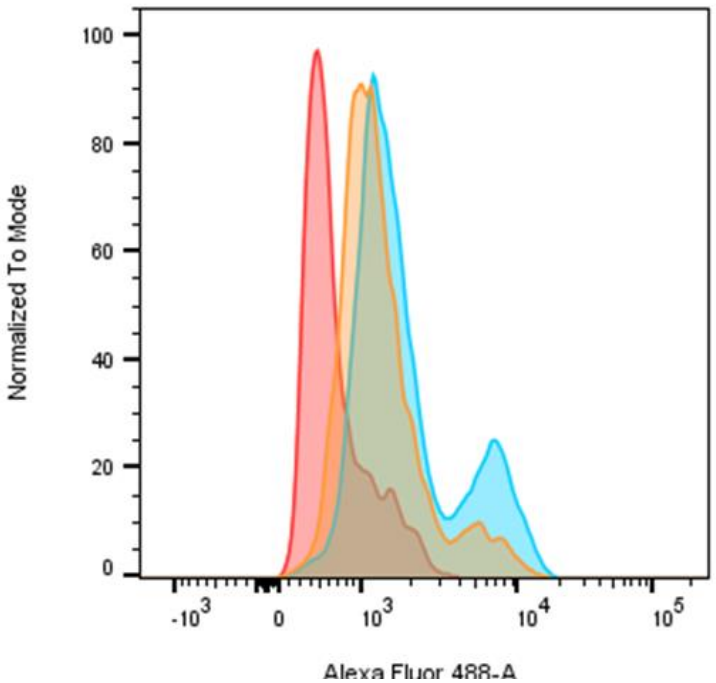

Figure 24. Click-IT assay. Red: shLUC + flavopiridol, Blue: shLUC, Orange: shLUC. Samples were normalized using the Modal option which scales all channels as a percentage of the maximum count. Flow cytometry data were analyzed with FlowJo. There is a slight decrease in nascent RNA upon PPME1 KD.

At this stage, we decided to perform a steady-state RNA-seq experiments on shLUC and shPPME1 to get a deeper understanding of the impact of PPME1 depletion on gene expression. First, we performed PCA to assess the clustering of our samples (Fig. 25 A).

The observation from our volcano plots is intriguing. When we noticed an increase in gene expression upon PPME1 depletion and a decrease in gene expression with LCMT1 depletion, it suggested us that these two proteins are indeed having antagonistic roles in gene regulation (Fig. 25 B). Further analysis of the specific genes affected by PPME1 depletion and LCMT1 depletion, as well as their downstream pathways, can provide more insights into their respective functions and how they interact in the regulation of transcription.

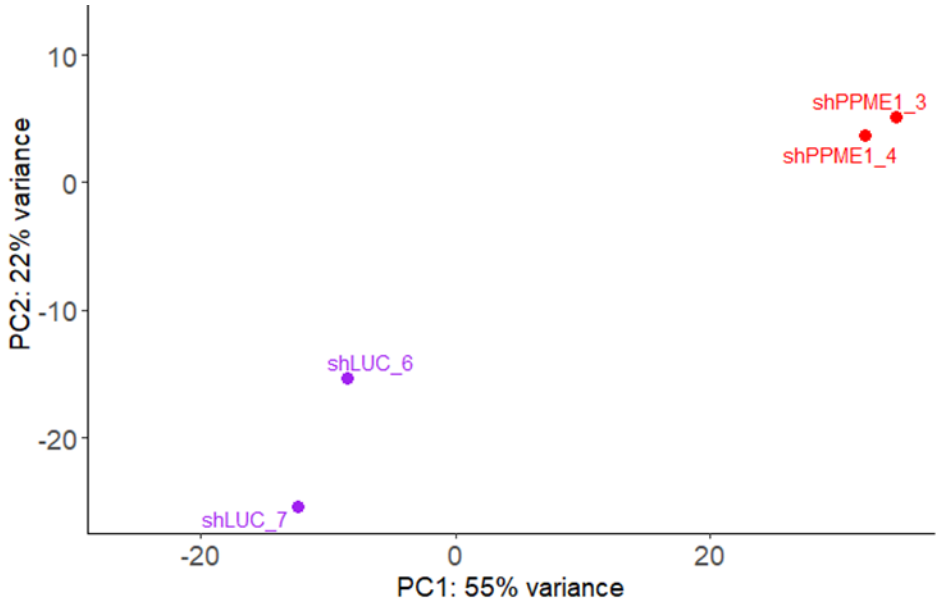
10
0
-10
-20
PC2: 22% variance
shPPME1_3
shPPME1_4
shLUC_6
shLUC_7
-20
0
20
PC1: 55% variance

A

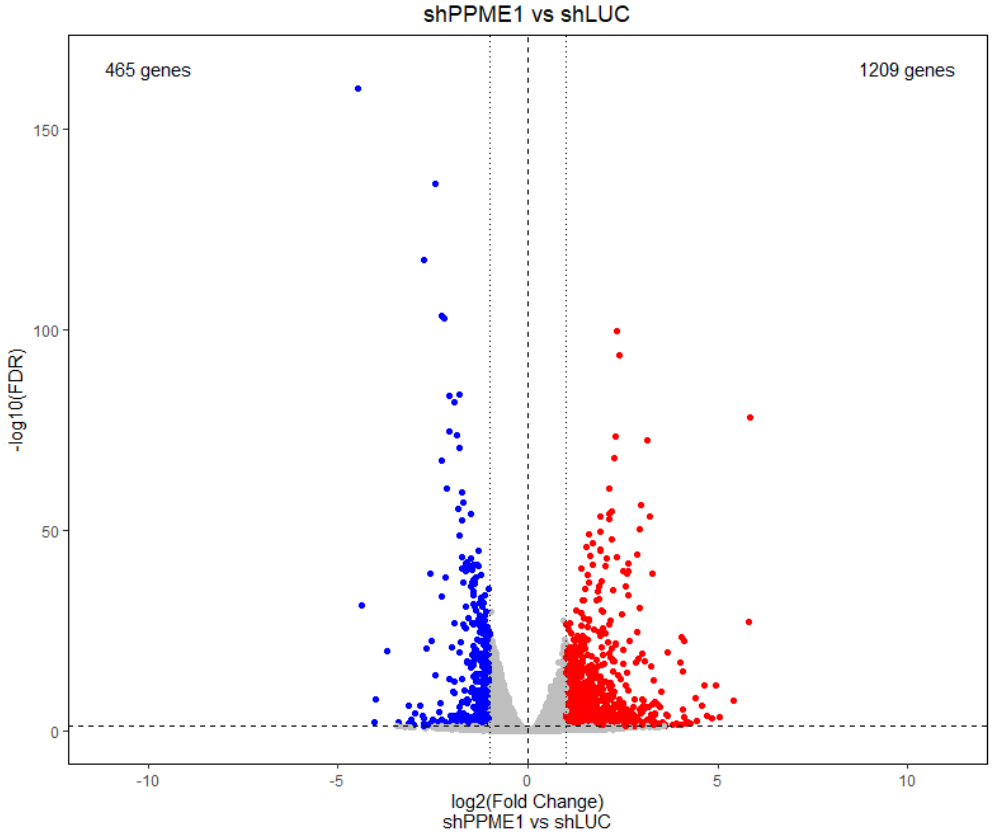
shPPME1 vs shLUC
465 genes
1209 genes
150
100
50
0
-log10(FDR)
-10
-5
0
5
10
log2(Fold Change)
shPPME1 vs shLUC

B

Figure 25. (A) PCA of shLUC and shPPME1 (2 replicates). (B) Volcano plot of shPPME1 (red dots on the right) vs shLUC (blue dots on the left) total RNA-seq. There is not such a drastic increase or decrease in gene expression upon PPME1 depletion.

Aware of how much PPME1 depletion can affect gene expression, we decided to continue its investigation performing ChIP-seq with Proteintech PPME1 antibody in WT HeLa cells (3 replicates). The discovery that PPME1 could bind to chromatin, particularly at the 3' end of genes following the RNA Polymerase II binding profile, suggested a potential role in transcriptional termination or post-transcriptional processes (Fig. 26 A).

We used HOMER software to analyze PPME1 binding motifs to understand the specific DNA sequence elements that PPME1 interacts with. Using HOMER, we were also able to observe that PPME1 binds both promoters and enhancers (72% promoters and 28% enhancers) (Fig. 26 B-C-D).

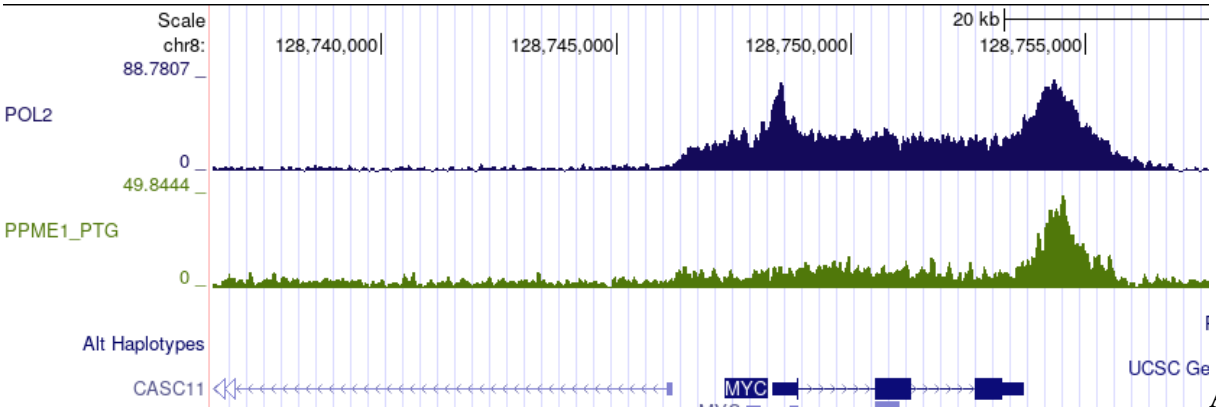

A

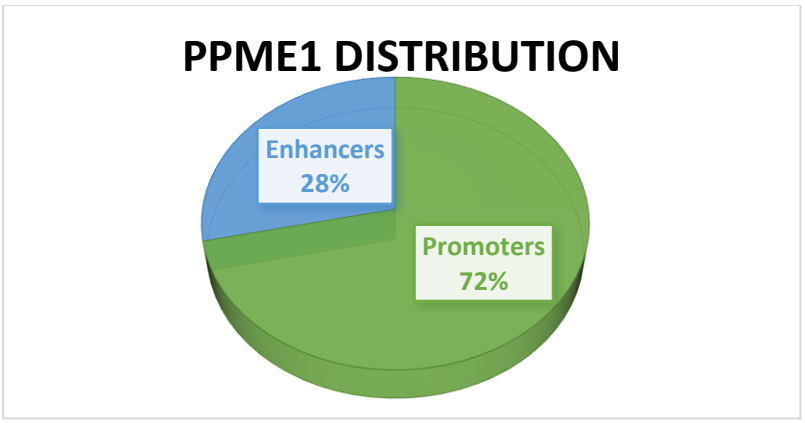

B

Motif	P-value	log P-pvalue	% of Targets	% of Background	STD(Bg STD)	Best Match/Details
	1e-174	-4.013e+02	45.70%	12.00%	50.8bp (76.0bp)	Elk1(ETS)/Hela-Elk1-ChIP-Seq(GSE31477)/Homer(0.956) More Information | Similar Motifs Found
	1e-66	-1.524e+02	7.81%	0.60%	56.3bp (78.4bp)	PRDM10(Zf)/HEK293-PRDM10.eGFP-ChIP-Seq(Encode)/Homer(0.812) More Information | Similar Motifs Found
	1e-29	-6.883e+01	70.44%	53.81%	56.2bp (79.0bp)	HINFP/MA0131.2/Jaspar(0.686) More Information | Similar Motifs Found
	1e-26	-6.034e+01	14.04%	5.49%	53.3bp (78.4bp)	ZBED1/MA0749.1/Jaspar(0.752) More Information | Similar Motifs Found

C

Motif	Name	P-value	log P-pvalue	q-value (Benjamini)	# Target Sequences with Motif	% of Targets Sequences with Motif
	Elk4(ETS)/Hela-Elk4-ChIP-Seq(GSE31477)/Homer	1e-159	-3.663e+02	0.0000	507.0	44.47%
	Elk1(ETS)/Hela-Elk1-ChIP-Seq(GSE31477)/Homer	1e-148	-3.412e+02	0.0000	486.0	42.63%
	ELF1(ETS)/Jurkat-ELF1-ChIP-Seq(SRA014231)/Homer	1e-131	-3.018e+02	0.0000	438.0	38.42%
	ETS(ETS)/Promoter/Homer	1e-130	-3.001e+02	0.0000	342.0	30.00%

D

Figure 26. The picture (A) shows a ChIP-seq track obtained from Genome Browser. RNA Polymerase is in blue, while PPME1 Proteintech ChIP-seq is in green. Most PPME1 is found at the 3' of the gene (MYC). (B) PPME1 if found at promoters (72%) and enhancers (28%). (C and D) HOMER motif analysis, known and de novo, respectively.

To confirm the presence and co-localization of PPME1 and RNA Polymerase II within the nucleus, we performed immunofluorescence experiments using a rabbit PPME1 and a mouse RNA Polymerase II antibodies. The observation that PPME1 was present in both the nucleus and cytoplasm aligned with the earlier findings from Western blot (WB). The key finding was the co-localization of PPME1 with RNA Polymerase II in the nucleus (Fig. 27). This suggested that these two proteins are likely interacting and working together within the same cellular compartment,

reinforcing the idea that PPME1 plays a role in transcription regulation, potentially influencing RNA Polymerase II activity.

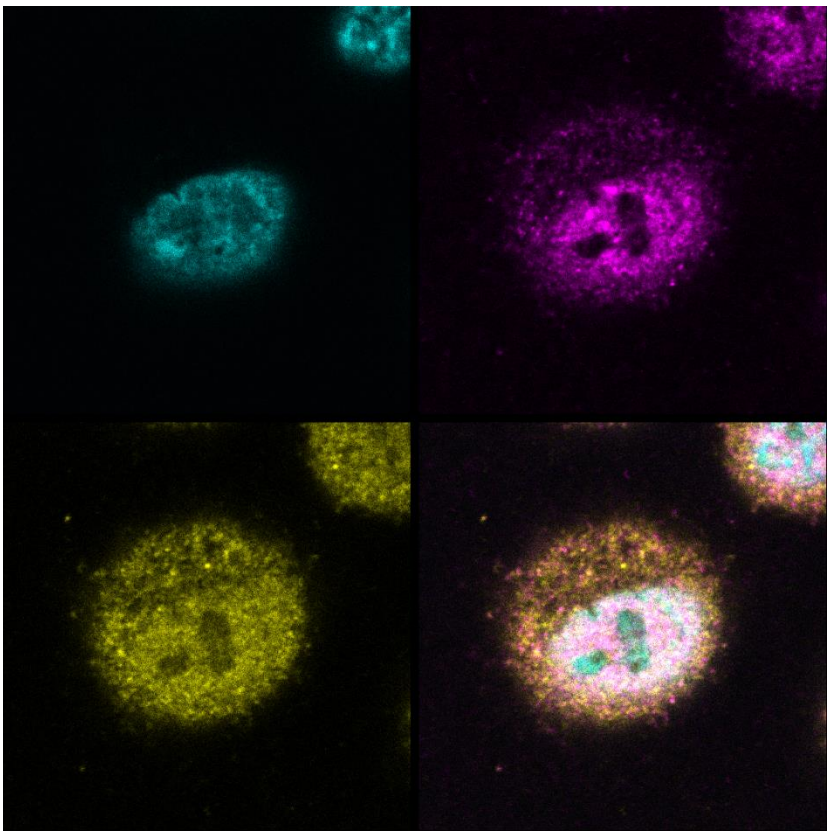

Figure 27. DAPI: Top left, RNA Polymerase II: Top right, PPME1: Bottom left, merge: bottom right.

Unfortunately, so far, we do not have any other experiments showing the mechanism of PPME1 binding and recruitment to the chromatin.

The questions we have been wondered at this point were: Why is PPME1 binding the chromatin? Does it have any other role in transcription/post transcription processes?

We assess that through a proteomic approach, going to investigate which kind of proteins bind PPME1 most in nucleus. We performed an IP in WT HeLa cells using the same antibody used for ChIP-seq. The elution was used both to check the IP efficacy (Fig. 28 A) and for MS run.

The presence of proteins related to RNA splicing, cleavage, and polyadenylation within the PPME1 binding partners suggested that PPME1 could be involved in the regulation of these processes. It implies that PPME1 might play a role in influencing RNA maturation (Fig. 28 B – C).

While this data suggests a correlation between PPME1 and RNA maturation, further experiments are needed to understand the exact mechanisms and functions of PPME1 in these processes. It would be beneficial to perform additional experiments to confirm and characterize these interactions and elucidate the specific roles of PPME1 in RNA maturation.

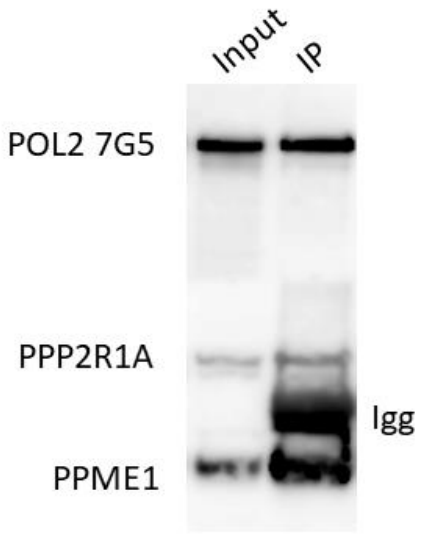

A

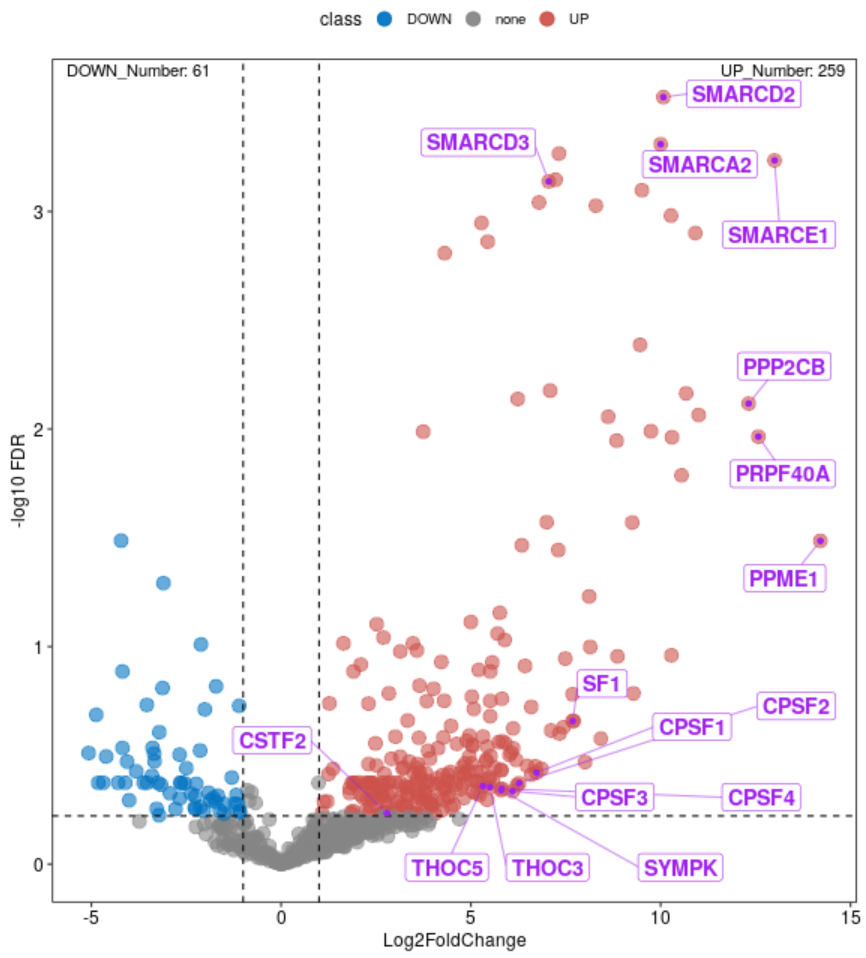

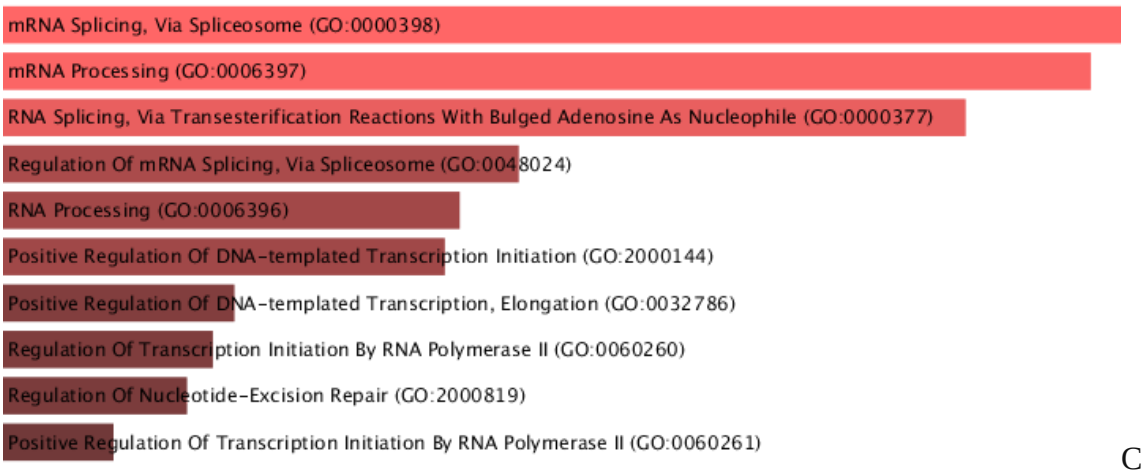

Figure 28. The WB (A) represents PPME1 IP in nucleus. Membrane was incubated with PPME1 ab, PPP2R1A (being one of the PP2A subunits we know for sure it binds PPME1), and RNA Polymerase II 7G5 ab. The plot shown above

(B) represents nuclear PPME1 IP (red dots on the right) vs nuclear Igg IP (blue dots on the left). The gene ontology (C) of proteins interacting with PPME1 with Foldchange >2 was made using Enrich website The first pathway coming out is related to RNA processing (CPSF1, CPSF2, CPSF3 etc), maturation and splicing (SF1, SYMPK, PRPF40A). There is another interesting cluster which comes out at the 6th position which is related to the chromatin remodeling (npBAF complex, such as SMARCD3, SMARCD2, SMARCE etc).

Chapter 3

Methods

Cell lines

Henrietta Lacks (HeLa) cells were cultured at 37°C and 5% CO_2 in Dulbecco's Modified Eagle's medium (DMEM: ThermoFisher Scientific) supplemented with 10% fetal bovine serum (FBS) and 1% L-glutamine (Corning). Human embryonic kidney (HEK) 293T cells (used for generation of lentiviruses) were cultured at 37°C and 5% CO_2 in DMEM supplemented with 10% FBS and 1% L-glutamine. LCMT1 KO 293T cells were gifted by Irfan's lab (University of Pennsylvania). They were cultured at 37°C and 5% CO_2 in DMEM supplemented with 10% FBS and 1% L-glutamine.

Infection of HeLa cells

Vectors pLKO.1-shLCMT1 and pLKO.1-shPPME1 were bought from the Wistar Institute screening facility. Vectors pLV-FLAG-HA-LCMT1_WT_shPROOF, pLV-FLAG-HA-LCMT1_R73A_shPROOF were obtained by VectorBuilder. All shRNAs and pLV plasmids were sequenced with plasmidsaurus. For infection, lentiviral particles were produced in HEK293T cells. HeLa were double infected: they were incubated with virus plus polybrene for 4-6 h, washed with PBS and incubated with growing media for 2-4 h and then incubated again with virus plus polybrene overnight. The following day virus media was replaced by growing media and the day after cells were selected with 2µg/mL puromycin. After 72 h selection, cells were harvested.

Reagents

Flavopiridol was purchased from Sigma-Aldrich (F3055) and reconstituted in DMSO. Biotin was purchased from Sigma-Aldrich (B4501-1G) and reconstituted in ammonium hydroxide. EU (5-Ethynyl Uridine) was purchased from Thermo Fisher (E10345) and reconstituted in H20.

SDS-PAGE and Immunoblotting

Collected treated cells were washed twice with cold PBS and lysed in ChIP lysis buffer (150 mM NaCl, 1% Triton X-100, 0.7% SDS, 500 mM DTT, 10 mM Tris-HCl, 5 mM EDTA) supplemented with 1 µg/mL aprotinin, 1 µg/mL leupeptin and 1 µg/mL pepstatin for 25 min. Lysed cells were centrifuged for 15 min at 14000 RPM at 4 ̊C. Laemmli lysis buffer (60mM Tris-HCl pH 6.8, 10% (v/v) glycerol, 2% (w/v) SDS) was added to protein extracts for 5 minutes at 95°C and protein concentration was determined using the Pierce BCA Protein Assay Kit. Proteins were loaded into Bolt 4 – 12% Bis Tris Plus gels and separated through gel electrophoresis (SDS-PAGE) in Bolt MES running buffer. Loaded proteins were transferred to Immunoblot PVDF membranes which were incubated with 10% BSA in TBST for 1h at room temperature. Primary incubation occurred at room temperature for 2 hours, or at 4 ̊C overnight. Membranes were washed twice with TBST for 15 minutes and then incubated with anti-mouse or anti-rabbit secondary antibody (1:10000 in 5% BSA in 1X TBST) for 1 hour at room temperature. Membranes were washed twice with TBST and visualized using Clarity Western ECL with LAS-3000 Imager.

Sample preparation for IP-MS

For Co-immunoprecipitation experiments, HeLa cells were collected and centrifuged at 3000 RPM for 8 minutes at 4 ̊C. The pellet was washed twice in cold PBS. Cells were resuspended in 5 volumes of Buffer A (10mM Tris pH 7.9, 1.5mM MgCl2, 10mM KCl, 0.5mM DTT, 1 mg/ml each of protease inhibitors aprotinin, leupeptin, and pepstatin) and incubated at 4 ̊C for 10 minutes rotating. They were centrifuged at 2000 RPM for 10 minutes and the cell pellet was resuspended in 2 volumes of Buffer A and homogenized with B pestle (10-15 strokes). The lysate was spun down at 2500 RPM for 10 minutes. The supernatant was kept as Cytoplasmic Extract. The pellet was resuspended in 1 volume of Buffer C (20mM Tris pH 8.0, 1.5mM MgCl2, 0.42M NaCl, 25% glycerol, 0.2mM EDTA, 0.5mM DTT, protease inhibitors) and homogenized with pestle B before rotating at 4 ̊C for 30 minutes. The lysate was centrifuged at 4 ̊C at 12000 RPM for 30 minutes. The supernatant was kept as Nuclear Extract. Both nuclear and cytoplasmic extracts were dialyzed against 2-4 L of BC80 (20mM Tris pH 8.0, 80mM KCl, 0.2mM EDTA, 10% glycerol, 1mM B-

mercaptoethanol, 0.2mM phenylmethylsulfonyl fluoride (PMSF) for 16 hours at 4 ̊C. Dialyzed samples were spun down at 1500 RPM for 20 minutes and stored at -80 after being frozen with liquid nitrogen.

IP followed by Mass spectrometry

For each IP-MS, 1.5 mg of nuclear or cytoplasmic extracts was used. 70 uL of Beads A or G were washed with 1 ml of Co-IP buffer (20 mM Tris pH 7.9, 100 mM NaCl, 0.1% NP-40 + protease inhibitors) and then incubated with lysate and 6 ug of antibody rotating at 4 ̊C for 2 hours. Beads were washed 3 times with 1 volume of Co-IP buffer and once with PBS + 0.05% NP-40. Proteins bound to the beads were eluted with 0,1 M glycine pH 3 (IgG elution Buffer) while shaking on the thermocycler at 1200 RPM at room temperature for 2 minutes. Tris-HCl pH 9.5 was added to eluate to neutralize pH. Eluates were prepared for SDS-PAGE and run on a 12-well Novex WedgeWell 10% Tris-Glycine Gel (Invitrogen) with Tris-Glycine-SDS buffer (Bio-Rad), at 100V for 10-15 minutes. The gel was stained with Colloidal Blue staining kit (Invitrogen) overnight and processed at the proteomics facility at the Wistar Institute. The gel lanes were excised and digested by trypsin and analyzed by LC-MS/MS on a Q-Exactive Plus mass spectrometer. MS/MS spectra were searched with full tryptic specificity against the UniProt human database using the MaxQuant. The iBAQ values were normalized to the total levels of the protein that was pulled down. Perseus was used to analyze mass spec data. iBAQ values were filtered based on contaminants and then transformed into log10. A two-sample t-test was used to test if the two or more samples were equal or not. A table with – Log Student's T-test p-value and Student's T-test difference was obtained.

TiO_2 phosphoproteome enrichment

1-2 mg of nuclear and cytoplasmic extracts (see 'sample preparation for IP-MS') were dialyzed against 8M Urea, 50mMTris, 20mM Glycine, 150mM NaCl, Phosphatase Inhibitors (1 M NaF, 50 mM beta-glycerophosphate, 50 mM Na3VO4) and Protease inhibitors, pH 8. Samples were

processed at the proteomics facility at the Wistar Institute. Samples were processed with Titanshpere Phos-TiO Kit from GL Sciences 5010-21311 3mg/200ul. 1 mg of dried sample was dissolved in 150 ul of Solution B (Lactic acid) and kept on ice. The column was prepared as follows: 20 ul of Buffer A (1ml 2% TFA + 4ml Acetonitrile) was added to the column and was centrifuged at 3000g for 2 minutes at RT. 20 ul of Buffer B (1 ml Solution B + 3ml Buffer A), was added to the column and then was centrifuged at 3000g for 2 minutes at RT. The samples were added to the column, centrifuged for 1000g for 10 minutes at RT. The flowthrough was taken and was reapplied to the column and spun for 1000g for 10 minutes at RT. The unbound was saved and kept on ice. The column was washed with 40 ul of Buffer B, spun at 6500 RPM for 2 minutes at RT. Column was washed with 40 ul of Buffer A, spun for 2 minutes at RT at 6500 RPM. This step was repeated twice. For elution, the column was places in a new 1.5ml collection tube and 50ul of 5% NH4OH was added and then centrifuged at 3500g for 5 minutes at RT. 50 ul of 5% Pyrrolidine was added and spun at 3500 RPM for 5 minutes at RT into the same tube. The same procedure was repeated on a new column using the saved Unbound material. Samples were resuspended in 25ul of 3% CAN, 2% FA and 8 ul were injected.

Chromatin Immunoprecipitation Sequencing (ChIP-Seq)

HeLa and 293T cells were cross-linked at room temperature for 5 minutes with 1% formaldehyde with mild rotation. To quench the cross-linking reaction 0.125 M glycine was added and cells were incubated again for 5 min at room temperature and then centrifuged for 5 min at 4 C at 1300 RPM. Cell pellet was washed twice with cold PBS and centrifuged for 5 minutes at 1300 RPM. Pellets were frozen in dry ice and stored at -80 (at least overnight). Frozen pellet was resuspended in 900 ul ChIP Buffer (150 mM NaCl, 1% TritonX-100, 5 mM EDTA, 10 mM Tris-HCl 7.5, 0.5 mM DTT) + 1ul/ml protease inhibitors (aprotinin, leupeptin, pepstatin) + 0.7-0.8% SDS and sonicated for 5-6 min using the Covaris S2 instrument (20% Duty Cycle, 1000 cycles/burst, 10 intensity). After sonication, 20 uL of each sonicated sample was brought to 100 uL with TE/SDS1% + 5ul of proteinase K (20mg/ml) and RNAse and was digested at 65C for 1h. Samples were then purified with Wizard PCR Clean up and the fragmented chromatin was checked by Tapestation. For each immunoprecipitation, diluted chromatin was incubated overnight at 4C with Proteins A or G Dynabeads (ThermoFisher), 10-20 ug of antibody, 2ug Drosophila Spike-in antibody and

drosophila chromatin got from 2 x 10^6 formaldehyde-crosslinked *D. melanogaster* S2 cells. Post-incubation, Dynabeads were washed twice with Mixed Micelle Wash Buffer (150 mM NaCl, 20 mM Tris-HCl pH 8, 5 mM EDTA, 65% w/v stock sucrose, 20% TritonX-100, 20% SDS), twice with Buffer500 (0.1% deoxycholate, 500 mM NaCl, 1M Hepes pH 7.5, 1mM EDTA, 1% TritonX-100), twice with LiCl/detergent was (0.5% deoxycholate, 250 mM LiCl, 1mM EDTA, 0.5% IGEPAL CA-630, 10 mM TrisCl pH 8.0) and once with TE buffer (10 mM Tris-HCl pH 7.5, 1mM EDTA). The beads were resuspended with 240 uL TE + SDS 1% and incubated at 65 C for 10 min in a thermomixer (rotate at 1200 RPM). Elution was repeated twice, and the collected aliquots were reverse cross-linked at 65 C overnight. 300 ug/mL Proteinase-K was added for 1h at 65C and then the DNA was isolated using the Zymogen ChIP DNA Clean and Concentrator Kit (Zymo Research D5205). DNA concentration was quantified by Qubit. Sequencing libraries were prepared using NEBNext Ultra II DNA Library Prep Kit and 200-500 base-pair size selection was performed using a Pippin Prep System and sequenced on an Illumina NextSeq 500 or NextSeq 2000. Sequenced reads were aligned to the Hg19 human or dm3 D. melanogaster reference genome using Burrows Wheeler Alignment tool (BWA) with the MEM algorithm and the generated files were converted to BAM files using Samtools which was also used to remove PCR duplicates (rndup) from BAM files and converted them to BigWig files. MACS2 was used for peak calling. Average read density across defined genomic intervals was computed using the Deeptools computeMatrix function. Data was visualized in RStudio with ggplot2 (v4.1.2) and ggrepel packages. Traveling ratio was calculated considering the coverage of RNA Polymerase II at the TSS and comparing it to the coverage at the gene body through TES.

Antibodies used for ChIP-seq are: Anti-RNA Polymerase II, raised against the N-terminus of subunit B1, rabbit polyclonal, Anti-RNA Polymerase II subunit B1 (phospho-CTD Ser2), clone 3E10, rat monoclonal, Anti-RNA Polymerase II subunit B1 (phospho-CTD Ser5), clone 3E8, rat monoclonal, Anti-PPME1, mouse monoclonal.

Click-iT EU labeling nascent RNA assay

HeLa cells infected with Lentiviruses and treated with 2 uM flavopiridol, were labeled with 1mM ethynyl-uridine (EU) for 40 min. They were collected and washed with PBS twice before

fixation/permeabilization (0.5% paraformaldehyde, 0.2% Tween 20, 0.1% BSA, 0.1% Azide) at room temperature for 15 min. Cells were washed with PBS and incubated for 30 min with 86.5 uL Click-iT reaction buffer, 4 uL CuSO4 buffer, 0.125 uL Alexa Fluor-azide-488 and 10.3 uL Click-iT reaction buffer additive (Click-iT™ RNA Alexa Fluor™ 488 Imaging Kit). Cells were washed twice with 200 uL Click-iT rinse buffer and once with PBS. Pellets were resuspended in 250 uL PBS and analyzed by LSR-18 flow cytometer. Data was analyzed with FlowJo.

fastGRO

15-30 million of cells were collected, washed with cold PBS and resuspended in ice-cold Swelling Buffer (SB) (10 mM Tris-HCl pH 7.5, 2 mM MgCl2, 3 mM CaCl2), then GSB Buffer (swelling buffer + 10% glycerol), lysed in Lysis Buffer (swelling buffer + 10% glycerol + NP40) and nuclei were frozen in Freezing buffer (FB) (40% glycerol, MgCl2, 0.1 mM EDTA, 50 mM Tris-HCl pH 7.8). Nuclei were labelled with 500 μM 4-thiouridine (4sU) for 30 minutes and lysed in TRIzol. *D.melanogaster* S2 cells (20×10^6) were also labelled with 4sU. 1/5 of chloroform was added to the lysate and after centrifugation the aqueous phase was collected. Isopropanol was used to precipitate RNA (room temperature for 10 min) and the pellet was washed twice with 75% ethanol and spun down (4 C, 12000 g for 10 min). The air-dry pellet was dissolved in 100 uL of H2O with 1:100 superase inhibitor and denaturated at 65 C for 10 minutes. 150 – 300 ug of RNA was sonicated (settings: 1 cycle: 30sec/30sec ON/OFF) and stored at -80 C overnight. The fragmentation efficiency was analyzed by Tapestation. RNA was incubated in the dark at 24˚C and 800 rpm for 2h with BB buffer (100 mM Tris pH 7.5, 10 mM EDTA), DMF and 300 ug of EZ-link HPDP biotin (Thermo Scientific). After incubation, the biotinylated RNA was supplemented with 800 uL of chloroform, centrifuged at 15000 rpm for 5 minutes and the upper phase was transferred into a new tube. 1/10 volume of NaCl and 1 volume of isopropanol were added. The reaction was centrifuged at 4 ˚C and 15000 rpm for 30 minutes and the pellet was then washed with ice-cold 75% ethanol. The RNA pellet was resuspended in 100 uL H2O and denaturated at 65C for 5 minutes. Labeled RNA was incubated with 100 uL of streptavidin beads (M-280) and incubated at 4 ˚C in rotation for 15 minutes. The beads were washed three times with 900 uL of pre-warmed to 65 C Wash buffer WB (100 mM Tris pH 7.5, 10 mM EDTA. 1M NaCl, 0.1% Tween-20) and three

times with room temperature WB. RNA was eluted twice using 100 uL of 100 mM DTT. RNA was purified with RNA Clean and Purification kit-5 (Zymo). RNA sequencing libraries were prepared using the NEBNext Ultra II Directional RNA Library Prep Kit for Illumina and 75 base-pair single-end reads were sequenced using the Illumina NEXTseq 500. Sequenced reads were aligned to the Hg19 human or dm3 D. melanogaster reference genome using BWA and BAM files were generated and processed as described for ChIP-seq. Deeptools was used to generate BigWig files which were then visualized in Genome Browser uscs. Average read density across defined genomic intervals was computed on the normalized BAM files using seqMINER 1.3.3 package with the following parameters: left and right extensions = 5.0 kb; internal bins = 160; flanking region bins = 20. Data was visualized in RStudio thanks to ggplot2 and ggrepel packages.

Total RNA-seq

HeLa were infected with shLUC, shLCMT1 and shPPME1 and selected for 3 days with puromycin before collecting them. Cells were lysed with 600 ul TRIzol and RNA was purified using Diret-zol RNA mini-prep kit (Zymo Research) with DNAse treatment. Barcoded RNA sequencing libraries were produced with the NEBNext Ultra Directional RNA Library Prep kit (New England Biolabs). RNA was sequenced on an Illumina NextSeq 2000 with 50bp paired end reads. QC was performed on FASTQ files using FASTQC. Read adapters were trimmed using cutadapt and aligned to the Hg19 human reference genome using STAR-2 v2.5 (quantMode TranscriptomeSAM --outFilterMultimapNmax 10 --outFilterMismatchNmax 10 --outFilterMismatchNoverLmax 0.3 --alignIntronMin 21 --alignIntronMax 0 --alignMatesGapMax 0 --alignSJoverhangMin 5 --runThreadN 12 --twopassMode Basic --twopass1readsN 60000000 --sjdbOverhang 100). BAM files were sorted and filtered based on alignment quality (q = 10) with Samtools v0.1.19. Feature counts are used to count mapped reads for genomic features such as genes and exons. DESeq2 was the tool used to identify differentially expressed genes using read counts normalized by feature length in RStudio 4.1.2. All plots were visualized with ggplot package.

pINTO-TurboID-INTS6-HF cloning and its expression in 293T cells

TurboID fragment was cloned into the vector pINTO-INTS6-HF using the Gibson cloning technique. TurboID was amplified by PCR with ccactagtccagtgtggtggatgaaagacaatactgtgcctctga (Forward) and tgctggatatctgcagaatt cttttcggcagaccgcagac (Reverse) primers. pINTO-INTS6-HF was digested for 1 h at 37C with EcoRI. Both vector and insert were loaded on an agarose gel for 25 min at 120 V and then purified by Wizard Gel Clean Up System kit (Promega) and their concentration was quantified via nanodrop. Two Gibson assembly reactions were set up as follows: 50 ng of the vector + 1:2 insert (or 1:3) + 10 ul Gibson reaction buffer. The reactions were left at 50 ̊C for 1 h and then 3.5 ul of the reaction was transformed into NEB5alpha bacteria, which were incubated at 37C overnight. Bacteria were miniprepped using PureYield Miniprep system (Promega) and plasmid was sequenced with Sanger sequencing.

293T cells were plated in 10 cm plates and transfected with 15 ug of the sequenced pINTO-TurboID-INTS6-HF plasmid.

Sample preparation for TurboID assay

20 ug of pINTO-TURBOID-INTS6-HF + 60 ul of lipofectamine2000 were transfected into 10 cm^3 293T. The following day, the zeocyn was added for 24h before starting the biotin (50 uM) treatment for 5 – 15 minutes. Cells were collected and proteins were extracted by ChIP Buffer. The increase of biotinylation was verified by WB using streptavidin-HRP antibody (abcam - ab7403).

TurboID Assay Enrichment

3 mg of extract was diluted in ChIP buffer and used for the biotinylation enrichment. 350 uL of magnetic beads (washed twice with ChIP buffer) were added to the extract and left rotating for 1 h at room temperature and then at 4 ̊C overnight. Beads were washed twice with 1 mL of ChIP buffer, once with 1M KCl, once with 1mL of 0.1 M Na_2CO3, once with 1ml of 2M urea in 10 mM Tris-HCl pH 8, twice with 1 mL of ChIP buffer. All washes (except Na_2CO3 and urea) had to be

performed at room temperature rotating or shaking for 2 minutes. The beads were boiled at 95 ̊C in 75 uL of 3X protein loading buffer supplemented with 20 mM DTT and 25 mM biotin for 10 minutes. Eluted proteins were collected with a magnetic rack. To check the efficiency of enrichment, 25 uL of eluted proteins were loaded into a SDS page gel and were checked by Western blot. The remaining 50 uL of elution was run on a 12-well Novex WedgeWell 10% Tris-Glycine Gel (Invitrogen) with Tris-Glycine-SDS buffer (Bio-Rad), at 100V for 10-15 minutes. The gel was stained with Colloidal Blue staining kit (Invitrogen) overnight and processed at the proteomics facility at the Wistar Institute (see IP-MS paragraph).

Immunofluorescence

Autoclaved coverslips were added to 24 well plates and then 50 000 HeLa cells were plated. On day 1, the coverslips were moved into a 6 well and left there until the end of the experiment. 1 mL of Fixative solution (4% formaldehyde in DPBS) per well and incubated at room temperature for 15 minutes. The fixative solution is removed and 1 ml of Permeabilization solution (0.5% Triton X-100 in DPBS) was added into each well and incubated for 15 minutes at room temperature. The Permeabilization Solution is removed and 1 ml of Block Solution (10% goat serum in DPBS) is added into each well and incubated 1 h at room temperature. The Blocking Solution is removed and 400 ul of primary antibody (diluted 1:50 – 1:100 in blocking solution) is added into each well and incubated at 4 ̊C overnight. The primary antibodies used are: RNA Polymerase II 8WG16 (ms), RNA Polymerase 4H8 (ms), RNA Polymerase 7G5 (ms) and PPME1 Proteintech (rb). Each RNA Polymerase II ab was incubated with PPME1 ab so that to have at the end 3 different combinations: RNA Polymerase II 8WG16 + PPME1, 4H8 + PPME1 and 7G5 + PPME1. Cells were rinsed three times with 1 ml of 1X DPBS for 1-2 minutes at room temperature. After washing, 1 ml of the secondary antibody (diluted 1:250-2:500 in Blocking Solution) was added into each well for 1h at room temperature. Cells were rinsed 3 times with 400 ul of wash buffer for 1-2 minute. Without removing the wash buffer, the coverslip was lifted with a needle and put on a small drop of mountain media with DAPI on a slide. Clear nail polish was used to help the coverslip to be glued to the slide. The slide was put at 4C overnight. The following day the slide was seen with the confocal microscopy.

Antibodies

Antibody	Source	Identifier
Anti - LCMT1 mouse monoclonal	Santa Cruz	Cat#sc-365221
Anti - PPME1 mouse monoclonal	Santa Cruz	Cat#sc-25278
Anti - PPP2R1A rabbit polyclonal	Proteintech	Cat#15882-1-AP
Anti - PPP2CA (clone 1D7) mouse monoclonal	Biolegend	Cat#824101
Anti - PPP2CA (clone 1D6) mouse monoclonal	Millipore, Sigma	Cat#05-421
Anti - PPP2CA rabbit polyclonal	Proteintech	Cat#13482-1-AP
Anti-RNA Polymerase II, clone CTD 4H8, mouse monoclonal	Millipore, Sigma	Cat#05-623
Anti-RNA Polymerase II CTD repeat YSPTSPS, clone 8WG16, mouse monoclonal	Santa Cruz	Cat#sc-56767
Anti-RNA Polymerase II subunit B1 (phospho-CTD Ser2), clone 3E10, rat monoclonal	Active motif	Cat#61984
Anti-RNA Polymerase II subunit B1 (phospho-CTD Ser5), clone 3E8, rat monoclonal	Active motif	Cat#61986
Anti-GAPDH, rabbit monoclonal	Cell Signaling Technologies	Cat#2118
Anti-DICE1 (INTS6), clone H-6, mouse monoclonal	Santa Cruz	Cat#sc-376524
Anti-INTS3, rabbit polyclonal	Proteintech	Cat#16620-1-AP
Anti-RNA Polymerase II, raised against the N-terminus of subunit B1, rabbit polyclonal	Alessandro Gardini, Wistar Institute, Philadelphia, PA 19104, USA	(Barbieri et al., 2018)
Anti- Drosophila H2Av, spike-in antibody	Active Motif	Cat#61686
Anti-Mouse IgG-HRP, horse polyclonal	Cell Signaling Technologies	Cat#7076
Anti-Rabbit IgG-HRP, goat polyclonal	Cell Signaling Technologies	Cat#7074
Anti-FLAG M2, mouse monoclonal	Sigma-Aldrich	Cat#: F1804
Streptavidin-HRP	Abcam	Cat#ab7403
Anti-mouse IgG, HRP-linked Antibody	Cell Signaling Technologies	Cat#7076S
Anti-rabbit IgG, HRP-linked Antibody	Cell Signaling Technologies	Cat#7074S
Anti-rat IgG, HRP-linked Antibody	Cell Signaling Technologies	Cat#7077S

Chapter 4

Future Directions

We have conducted a comprehensive series of experiments and have gained significant insights into the roles of PP2A methylation, LCMT1, and PPME1 in transcription and post-transcriptional processes. Our plans for additional experiments are well-considered and will provide further clarity on these complex mechanisms. Here is a brief summary of our proposed experiments:

- 1D6 antibody used for mass spectrometry in shLUC and shLCMT1 is known to recognize a little bit better the unmethylated form of PP2CA rather than the methylated one. We are pretty sure about our fundings, since all MS data we got were normalized to total PP2A pulled down. However, to confirm that the approach we used so far is not biased, we are planning to use a HeLa cell line overexpressing PPP2R1A-V5 tagged. Our plan is to infect that cell line with shLUC and shLCMT1 viruses, selected that for 3 days and performing IPs followed by mass spec with V5 antibody which will allow us to get unbiased mass spectrometry data;
- shLUC/shLCMT1 experiments showed that LCMT1 depletion caused an increase of RNA Polymerase II phosphorylation and nascent RNA, but a decrease in steady-state RNA. Our experiments, however, does not show why this is happening and the mechanism. Our first goal, hence, is to investigate LCMT1 role in post-transcriptional events such as RNA maturation. We are planning to perform a chromatin-associated RNA long-reads sequencing with nanopore to analyze splicing events. Our hypothesis is that the uncontrolled increase of transcription upon LCMT1 depletion, generates aberrant RNAs which being defective are degraded. Long-reads sequencing will help us know if LCMT1 KD is effectively causing all those maturation defects;
- Phosphoproteome results we showed are missing LCMT1 short-term depletion data. To have the chance to get more peptides, we would like to perform more replicates;
- PPME1 understanding role in transcription is not clear yet. First, we would like to study PPME1 dynamics in chromatin binding. Our beginning plan is to use a known PPME1

inhibitor, ABL-127, to see if a deactivated PPME1 is still able to bind the chromatin and in case, if the region bindings are different. In the future, we will be performing most of the experiments described in my thesis using ABL-127 as one of our conditions.

Chapter 5

Discussion

Regulating gene expression is crucial for maintaining proper cell function, and disruptions in these regulatory processes can contribute to various diseases, including cancer. RNA Polymerase II plays a central role in transcribing genes, and its regulation at each stage of transcription is highly orchestrated by various protein complexes. Dysregulation of these complexes can lead to abnormal upregulation of transcription, which is associated with the development of transcriptionally-addicted tumors.

One of the protein complexes involved in the regulation of RNA Polymerase II is the Integrator complex. Integrator is a large multi-subunit complex that plays a significant role in the control of gene expression. Dysfunctions in the Integrator complex have been identified in a variety of human cancers. Researchers, including those from the Gardini lab, have demonstrated that Integrator acts as a tumor suppressor in different cancer contexts by participating in the regulation of RNA Polymerase II.

A notable discovery in this context is that Integrator forms a complex with the PP2A (Protein Phosphatase 2A) phosphatase to regulate RNA Polymerase II pause-release and its transition into productive elongation. Importantly, this finding represents the first time that PP2A has been shown to directly regulate transcription. PP2A is a critical cellular enzyme responsible for dephosphorylating various proteins, and its involvement in transcriptional regulation underscores its importance in maintaining proper gene expression.

However, the roles and regulation of the Integrator complex and PP2A in the context of maintaining proper gene expression are still not fully understood. Further research in this area is essential to gain a comprehensive understanding of how these complexes function, how they are regulated, and how their dysfunction contributes to disease, especially cancer. Such knowledge could offer important insights for the development of therapeutic strategies to target these complexes and restore normal gene expression in cancer cells.

Investigating the role of PP2A methylation (which represents one of the ways to activate/deactivate the phosphatase) occurring at Leucine 309 of the catalytic subunit, in transcription is an important research direction. Methylation can have profound effects on its activity, stability, and interactions with other molecules, and understanding how this modification influences PP2A role in transcription can provide valuable insights into the regulation of gene expression.

To assess that, we first compared the phosphorylation status of transcription-related proteins substrate of PP2A when unmethylated PP2A levels increased or decreased. We found that PP2A-INT-RNA Polymerase II binding was not affected by methylation status of PP2A, on the contrary RNA Polymerase II CTD phosphorylation depended on PP2A form. We also, saw that when LCMT1 levels decrease, there is an increase in nascent RNA but a decrease in steady-state RNA. Our findings suggest an interesting connection between LCMT1 level downregulation and its impact on RNA Polymerase II phosphorylation, transcription activity, and nascent RNA production. The observation that depleting PPME1 leads to opposite results compared to LCMT1 depletion may reveal a complex regulatory interplay in the context of transcription and post-transcriptional processes. It is possible that LCMT1 and PPME1 play roles in modulating each other's effects. Depleting one may disrupt this balance, resulting in compensatory changes when the other is depleted.

RNA Polymerase pause-release is an important checkpoint for transcription regulation and skipping that process because of a hyper-phosphorylation of Serine 2 and 5 of CTD can be deleterious for the proper production of stable RNA and proper cell functions. Our findings may have important implications for understanding the molecular mechanisms underlying transcriptional regulation and how PP2A methylation can be a key player in these processes. Additionally, this research could lead to the development of targeted therapies that modulate PP2A methylation as a potential strategy for controlling aberrant transcription in diseases such as cancer.

REFERENCES

Amin, P., Awal, S., Vigneron, S., Roque, S., Mechali, F., Labbé, J. C., Lorca, T., & Castro, A. (2022). PP2A-B55: substrates and regulators in the control of cellular functions. In *Oncogene* (Vol. 41, Issue 1). https://doi.org/10.1038/s41388-021-02068-x

Barbieri, E., Hill, C., Quesnel-Vallières, M., Zucco, A. J., Barash, Y., & Gardini, A. (2020). Rapid and Scalable Profiling of Nascent RNA with fastGRO. *Cell Reports*, *33*(6). https://doi.org/10.1016/j.celrep.2020.108373

Barbieri, E., Trizzino, M., Welsh, S. A., Owens, T. A., Calabretta, B., Carroll, M., Sarma, K., & Gardini, A. (2018). Targeted Enhancer Activation by a Subunit of the Integrator Complex. *Molecular Cell*, *71*(1). https://doi.org/10.1016/j.molcel.2018.05.031

Dacol, E. C., Wang, S., Chen, Y., & Lepique, A. P. (2021). The interaction of SET and protein phosphatase 2A as target for cancer therapy. In *Biochimica et Biophysica Acta - Reviews on Cancer* (Vol. 1876, Issue 1). https://doi.org/10.1016/j.bbcan.2021.188578

Drouin, S., Laramée, L., Jacques, P. É., Forest, A., Bergeron, M., & Robert, F. (2010). DSIF and RNA polymerase II CTD phosphorylation coordinate the recruitment of Rpd3S to actively transcribed genes. *PLoS Genetics*, *6*(10). https://doi.org/10.1371/journal.pgen.1001173

Frohner, I. E., Mudrak, I., Kronlachner, S., Schüchner, S., & Ogris, E. (2020). Antibodies recognizing the C terminus of PP2A catalytic subunit are unsuitable for evaluating PP2A activity and holoenzyme composition. *Science Signaling*, *13*(616). https://doi.org/10.1126/scisignal.aax6490

Frohner, I. E., Mudrak, I., Schüchner, S., Anrather, D., Hartl, M., Sontag, J. M., Sontag, E., Wadzinski, B. E., Preglej, T., Ellmeier, W., & Ogris, E. (2020). PP2AC Phospho-Tyr307 Antibodies Are Not Specific for this Modification but Are Sensitive to Other PP2AC Modifications Including Leu309 Methylation. *Cell Reports*, *30*(9). https://doi.org/10.1016/j.celrep.2020.02.035

Gardini, A., Baillat, D., Cesaroni, M., Hu, D., Marinis, J. M., Wagner, E. J., Lazar, M. A., Shilatifard, A., & Shiekhattar, R. (2014). Integrator regulates transcriptional initiation and

pause release following activation. *Molecular Cell*, *56*(1). https://doi.org/10.1016/j.molcel.2014.08.004

Guo, F., Stanevich, V., Wlodarchak, N., Li, Y., Pallas, D. C., Sengupta, R., Jiang, L., Satyshur, K. A., & Xing, Y. (2013). Structural basis of PP2A phosphatase activator reveals a unique chaperone function in PP2A activation. *The FASEB Journal*, *27*(S1). https://doi.org/10.1096/fasebj.27.1_supplement.1043.3

Heidemann, M., Hintermair, C., Voß, K., & Eick, D. (2013). Dynamic phosphorylation patterns of RNA polymerase II CTD during transcription. In *Biochimica et Biophysica Acta - Gene Regulatory Mechanisms* (Vol. 1829, Issue 1). https://doi.org/10.1016/j.bbagrm.2012.08.013

Janssens, V., Goris, J., & Van Hoof, C. (2005). PP2A: The expected tumor suppressor. In *Current Opinion in Genetics and Development* (Vol. 15, Issue 1). https://doi.org/10.1016/j.gde.2004.12.004

Jiang, L., Stanevich, V., Satyshur, K. A., Kong, M., Watkins, G. R., Wadzinski, B. E., Sengupta, R., & Xing, Y. (2013). Structural basis of protein phosphatase 2A stable latency. *Nature Communications*, *4*. https://doi.org/10.1038/ncomms2663

Kauko, O., Imanishi, S. Y., Kulesskiy, E., Yetukuri, L., Laajala, T. D., Sharma, M., Pavic, K., Aakula, A., Rupp, C., Jumppanen, M., Haapaniemi, P., Ruan, L., Yadav, B., Suni, V., Varila, T., Corthals, G. L., Reimand, J., Wennerberg, K., Aittokallio, T., & Westermarck, J. (2020). Phosphoproteome and drug-response effects mediated by the three protein phosphatase 2A inhibitor proteins CIP2A, SET, and PME-1. *Journal of Biological Chemistry*, *295*(13). https://doi.org/10.1074/jbc.RA119.011265

Kaur, A., & Westermarck, J. (2016). Regulation of protein phosphatase 2A (PP2A) tumor suppressor function by PME-1. *Biochemical Society Transactions*, *44*(6). https://doi.org/10.1042/BST20160161

Kirstein, N., Gomes Dos Santos, H., Blumenthal, E., & Shiekhattar, R. (2021). The Integrator complex at the crossroad of coding and noncoding RNA. In *Current Opinion in Cell Biology* (Vol. 70). https://doi.org/10.1016/j.ceb.2020.11.003

Kong, M., Ditsworth, D., Lindsten, T., & Thompson, C. B. (2009). α4 Is an Essential Regulator of PP2A Phosphatase Activity. *Molecular Cell*, *36*(1). https://doi.org/10.1016/j.molcel.2009.09.025

Lai, F., Gardini, A., Zhang, A., & Shiekhattar, R. (2015). Integrator mediates the biogenesis of enhancer RNAs. *Nature*, *525*(7569). https://doi.org/10.1038/nature14906

Li, Y., Balakrishnan, V. K., Rowse, M., Wu, C. G., Bravos, A. P., Yadav, V. K., Ivarsson, Y., Strack, S., Novikova, I. V., & Xing, Y. (2022). Coupling to short linear motifs creates versatile PME-1 activities in PP2A holoenzyme demethylation and inhibition. *ELife*, *11*. https://doi.org/10.7554/ELIFE.79736

Liu, H., Gu, Y., Wang, H., Yin, J., Zheng, G., Zhang, Z., Lu, M., Wang, C., & He, Z. (2015). Overexpression of PP2A inhibitor SET oncoprotein is associated with tumor progression and poor prognosis in human non-small cell lung cancer. *Oncotarget*, *6*(17). https://doi.org/10.18632/oncotarget.3818

Lyons, S. P., Greiner, E. C., Cressey, L. E., Adamo, M. E., & Kettenbach, A. N. (2021). Regulation of PP2A, PP4, and PP6 holoenzyme assembly by carboxyl-terminal methylation. *Scientific Reports*, *11*(1). https://doi.org/10.1038/s41598-021-02456-z

Moreno, R. Y., Juetten, K. J., Panina, S. B., Butalewicz, J. P., Floyd, B. M., Venkat Ramani, M. K., Marcotte, E. M., Brodbelt, J. S., & Zhang, Y. J. (2023). Distinctive interactomes of RNA polymerase II phosphorylation during different stages of transcription. *IScience*, *26*(9). https://doi.org/10.1016/j.isci.2023.107581

Nasa, I., & Kettenbach, A. N. (2020). Effects of carboxyl-terminal methylation on holoenzyme function of the PP2A subfamily. In *Biochemical Society Transactions* (Vol. 48, Issue 5). https://doi.org/10.1042/BST20200177

Ohe, S., Kubota, Y., Yamaguchi, K., Takagi, Y., Nashimoto, J., Kozuka-Hata, H., Oyama, M., Furukawa, Y., & Takekawa, M. (2022). ERK-mediated NELF-A phosphorylation promotes transcription elongation of immediate-early genes by releasing promoter-proximal pausing of RNA polymerase II. *Nature Communications*, *13*(1). https://doi.org/10.1038/s41467-022-35230-4

Palancade, B., & Bensaude, O. (2003). Investigating RNA polymerase II carboxyl-terminal domain (CTD) phosphorylation. In *European Journal of Biochemistry* (Vol. 270, Issue 19). https://doi.org/10.1046/j.1432-1033.2003.03794.x

Phatnani, H. P., & Greenleaf, A. L. (2006). Phosphorylation and functions of the RNA polymerase II CTD. In *Genes and Development* (Vol. 20, Issue 21). https://doi.org/10.1101/gad.1477006

Sablina, A. A., & Hahn, W. C. (2007). The role of PP2A A subunits in tumor suppression. In *Cell adhesion & migration* (Vol. 1, Issue 3). https://doi.org/10.4161/cam.1.3.4986

Schüller, R., Forné, I., Straub, T., Schreieck, A., Texier, Y., Shah, N., Decker, T. M., Cramer, P., Imhof, A., & Eick, D. (2016). Heptad-Specific Phosphorylation of RNA Polymerase II CTD. *Molecular Cell*, *61*(2). https://doi.org/10.1016/j.molcel.2015.12.003

Sents, W., Ivanova, E., Lambrecht, C., Haesen, D., & Janssens, V. (2013). The biogenesis of active protein phosphatase 2A holoenzymes: A tightly regulated process creating phosphatase specificity. In *FEBS Journal* (Vol. 280, Issue 2). https://doi.org/10.1111/j.1742-4658.2012.08579.x

Seshacharyulu, P., Pandey, P., Datta, K., & Batra, S. K. (2013). Phosphatase: PP2A structural importance, regulation and its aberrant expression in cancer. In *Cancer Letters* (Vol. 335, Issue 1). https://doi.org/10.1016/j.canlet.2013.02.036

Shi, Y. (2009). Serine/Threonine Phosphatases: Mechanism through Structure. In *Cell* (Vol. 139, Issue 3). https://doi.org/10.1016/j.cell.2009.10.006

Stanevich, V., Jiang, L., Satyshur, K., Li, Y., Jeffrey, P., Li, Z., Menden, P., Semmelhack, M., & Xing, Y. (2013). Structural insights into tight control of PP2A methylation and function by LCMT-1. *The FASEB Journal*, *27*(S1). https://doi.org/10.1096/fasebj.27.1_supplement.1043.6

Stanevich, V., Jiang, L., Sengupta, R., Satyshur, K., Watkins, G., Wadzinski, B., Kong, M., & Xing, Y. (2013). Structural basis of stable PP2A latency by α4-protein. *The FASEB Journal*, *27*(S1). https://doi.org/10.1096/fasebj.27.1_supplement.1043.5

Stanevich, V., Zheng, A., Guo, F., Jiang, L., Wlodarchak, N., & Xing, Y. (2014). Mechanisms of the scaffold subunit in facilitating protein phosphatase 2A methylation. *PLoS ONE*, *9*(1). https://doi.org/10.1371/journal.pone.0086955

Tellier, M., Zaborowska, J., Neve, J., Nojima, T., Hester, S., Fournier, M., Furger, A., & Murphy, S. (2022). CDK9 and PP2A regulate RNA polymerase II transcription termination and coupled RNA maturation . *EMBO Reports*, *23*(10). https://doi.org/10.15252/embr.202154520

Tian, H., Lu, Y., Liu, J., Liu, W., Lu, L., Duan, C., Gao, G., & Yang, H. (2018). Leucine carboxyl methyltransferase downregulation and protein phosphatase methylesterase upregulation contribute toward the inhibition of protein phosphatase 2A by α-synuclein. *Frontiers in Aging Neuroscience*, *10*(JUN). https://doi.org/10.3389/fnagi.2018.00173

Vervoort, S. J., Welsh, S. A., Devlin, J. R., Barbieri, E., Knight, D. A., Offley, S., Bjelosevic, S., Costacurta, M., Todorovski, I., Kearney, C. J., Sandow, J. J., Fan, Z., Blyth, B., McLeod, V., Vissers, J. H. A., Pavic, K., Martin, B. P., Gregory, G., Demosthenous, E., … Johnstone, R. W. (2021). The PP2A-Integrator-CDK9 axis fine-tunes transcription and can be targeted therapeutically in cancer. *Cell*, *184*(12). https://doi.org/10.1016/j.cell.2021.04.022

Wang, X., Bajaj, R., Bollen, M., Peti, W., & Page, R. (2016). Expanding the PP2A Interactome by Defining a B56-Specific SLiM. *Structure*, *24*(12). https://doi.org/10.1016/j.str.2016.09.010

Washburn, R. S., & Gottesman, M. E. (2015). Regulation of transcription elongation and termination. In *Biomolecules* (Vol. 5, Issue 2). https://doi.org/10.3390/biom5021063

Welsh, S. A., & Gardini, A. (2023). Genomic regulation of transcription and RNA processing by the multitasking Integrator complex. In *Nature Reviews Molecular Cell Biology* (Vol. 24, Issue 3). https://doi.org/10.1038/s41580-022-00534-2

Wlodarchak, N., & Xing, Y. (2016). PP2A as a master regulator of the cell cycle. In *Critical Reviews in Biochemistry and Molecular Biology* (Vol. 51, Issue 3). https://doi.org/10.3109/10409238.2016.1143913

Wu, C. G., Chen, H., Guo, F., Yadav, V. K., McIlwain, S. J., Rowse, M., Choudhary, A., Lin, Z., Li, Y., Gu, T., Zheng, A., Xu, Q., Lee, W., Resch, E., Johnson, B., Day, J., Ge, Y., Ong, I. M., Burkard, M. E., … Xing, Y. (2017). PP2A-B′ holoenzyme substrate recognition, regulation and role in cytokinesis. *Cell Discovery*, *3*. https://doi.org/10.1038/celldisc.2017.27

Wu, C. G., Zheng, A., Jiang, L., Rowse, M., Stanevich, V., Chen, H., Li, Y., Satyshur, K. A., Johnson, B., Gu, T. J., Liu, Z., & Xing, Y. (2017). Methylation-regulated decommissioning of multimeric PP2A complexes. *Nature Communications*, *8*(1). https://doi.org/10.1038/s41467-017-02405-3

Xu, Y., Xing, Y., Chen, Y., Chao, Y., Lin, Z., Fan, E., Yu, J. W., Strack, S., Jeffrey, P. D., & Shi, Y. (2006). Structure of the Protein Phosphatase 2A Holoenzyme. *Cell*, *127*(6). https://doi.org/10.1016/j.cell.2006.11.033

Yabe, R., Tsuji, S., Mochida, S., Ikehara, T., Usui, T., Ohama, T., & Sato, K. (2018). A stable association with PME-1 may be dispensable for PP2A demethylation – implications for the detection of PP2A methylation and immunoprecipitation. *FEBS Open Bio*, *8*(9). https://doi.org/10.1002/2211-5463.12485

Yu, M., Yang, W., Ni, T., Tang, Z., Nakadai, T., Zhu, J., & Roeder, R. G. (2015). RNA polymerase II-associated factor 1 regulates the release and phosphorylation of paused RNA polymerase II. *Science*, *350*(6266). https://doi.org/10.1126/science.aad2338

Zheng, H., Qi, Y., Hu, S., Cao, X., Xu, C., Yin, Z., Chen, X., Li, Y., Liu, W., Li, J., Wang, J., Wei, G., Liang, K., Chen, F. X., & Xu, Y. (2021). Erratum: Identification of integrator-PP2A complex (INTAC), an RNA polymerase II phosphatase (Science DOI: 10.1126/science.abb5872). In *Science* (Vol. 371, Issue 6526). https://doi.org/10.1126/science.abg4122